JOURNAL OF GEOPHYSICAL RESEARCH, VOL. 106, NO. D23, PAGES 32,337-32,360, DECEMBER 16, 2001

Evolution of tropospheric ozone under anthropogenic activities and associated radiative forcing of climate

D. A. Hauglustaine[1]
Service d'Aéronomie du CNRS, Paris, France

G. P. Brasseur[2]
Max Planck Institute for Meteorology, Hamburg, Germany

Abstract. The budget of ozone and its evolution associated with anthropogenic activities are simulated with the Model for Ozone and Related Chemical Tracers (MOZART) (version 1). We present the changes in tropospheric ozone and its precursors (CH_4, NMHCs, CO, NO_x) since the preindustrial period. The ozone change at the surface exhibits a maximum increase at midlatitudes in the northern hemisphere reaching more than a factor of 3 over Europe, North America, and Southeast Asia during summer. The calculated preindustrial ozone levels are particularly sensitive to assumptions about natural and biomass burning emissions of precursors. The possible future evolution of ozone to the year 2050 is also simulated, using the Intergovernmental Panel on Climate Change IS92a scenario to estimate the global and geographical changes in surface emissions. The future evolution of ozone stresses the important role played by the tropics and the subtropics. In this case a maximum ozone increase is calculated in the northern subtropical region and is associated with increased emissions in Southeast Asia and Central America. The ozone future evolution also affects the more remote regions of the troposphere, and an increase of 10–20% in background ozone levels is calculated over marine regions in the southern hemisphere. Our best estimate of the global and annual mean radiative forcing associated with tropospheric ozone increase since the preindustrial era is 0.43 W m^{-2}. This value represents about 20% of the forcing associated with well-mixed greenhouse gases. The normalized tropospheric ozone radiative forcing is 0.048 W m^{-2} DU^{-1}. An upper estimate on our forcing of 0.77 W m^{-2} is calculated when a stratospheric tracer is used to approximate background ozone levels. In 2050 an additional ozone forcing of 0.26 W m^{-2} is calculated, providing a forcing from preindustrial to 2050 of 0.69 W m^{-2}.

1. Introduction

A comparison between ozone measurements made during the nineteenth century and those made in recent decades suggests that concentrations have been increasing in the troposphere since preindustrial times. This change is attibuted to growing emissions of precursors such as methane (CH_4), carbon monoxide (CO), nonmethane hydrocarbons (NMHCs), and nitrogen oxides (NO_x=NO+NO_2) [e.g., *Linvill et al.*, 1980; *Bojkov*, 1986; *Volz and Kley*, 1988]. Several studies based on two-dimensional (2-D) [*Hough and Derwent*, 1990; *Hauglustaine et al.*, 1994; *Forster et al.*, 1996] or three-dimensional (3-D) [*Crutzen and Zimmermann*, 1991; *Müller and Brasseur*, 1995] models have provided support for this hypothesis.

Since ozone absorbs both solar and infrared radiation, previous work has indicated a potentially significant contribution of tropospheric ozone increase to the radiative forcing of climate [*Fishman et al.*, 1979; *Wang and Sze*, 1980; *Ramanathan et al.*, 1985; *Dickinson and Cicerone*, 1986]. The first calculations of the radiative forcing of anthropogenically produced tropospheric ozone increase performed with 2-D models give a global mean forcing in the range 0.3–0.55 W m^{-2} [*Hauglustaine et al.*, 1994; *Forster et al.*, 1996]. The first estimates of the forcing derived from 3-D chemical transport models (CTMs) indicate a value in the range 0.28–0.5 W m^{-2} [*Lelieveld and van Dorland*, 1995; *Chalita*

[1]Also at Laboratoire des Sciences du Climat et de l'Environnement, Gif-sur-Yvette, France.

[2]Also at National Center for Atmospheric Research, Boulder, Colorado.

Paper number 2001JD900175.
0148-0227/01/2001JD900175$09.00

et al., 1996]. Although the variability in these estimates is substantial estimate (mainly due to different assumptions regarding, for example, the role of clouds, or the stratospheric temperature adjustment), there seems to be a consensus among previous studies that tropospheric O_3 provides a positive forcing (warming) on climate. No estimate of the tropospheric ozone forcing since the preindustrial period was reported in the early *Intergovernmental Panel on Climate Change* (*IPCC*) [1990, 1992] reports due to the lack of global estimates. However, based on initial model calculations and estimates by *Fishman* [1991] and *Marenco et al.* [1994], *IPCC* [1994, 1996] suggested for tropospheric ozone forcing a range of 0.2-0.6 W m^{-2}.

Since these early estimates, there has been a considerable effort devoted to the calculation of the tropospheric ozone forcing (preindustrial to present). For this purpose, studies have used global 3-D model ozone distributions [*Berntsen et al.*, 1997; *van Dorland et al.*, 1997; *Roelofs et al.*, 1997; *Stevenson et al.*, 1998; *Haywood et al.*, 1998; *Brasseur et al.*, 1998a; *Mickley et al.*, 1999; *Berntsen et al.*, 2000; *Lelieveld and Dentener*, 2000] or global O_3 observations [*Portmann et al.*, 1997; *Kiehl et al.*, 1999]. Similar protocols regarding the definition and calculation of the forcing have been adopted. These more recent studies provide a forcing in the range 0.28–0.44 W m^{-2}.

Emissions of ozone precursors are expected to increase significantly in the future. This is particularly the case in regions where rapid economic growth or population increase are expected (e.g., Southeast Asia, South and Central America, Africa) [*van Aardenne et al.*, 1999]. Several studies have pointed out the potentially important impact of Asian emissions on the background level of pollutants over the Pacific and northern United States [*Berntsen et al.*, 1996, 1999; *Jaffe et al.*, 1999; *Jacob et al.*, 1999; *Mauzerall et al.*, 2000]. Estimates of future levels of tropospheric ozone and associated radiative forcing have been performed with several models. A first estimate for year 2050, based on IPCC IS92a scenario, by *Chalita et al.* [1996] provided a forcing of 0.15 W m^{-2} relative to present. More recent estimates by *van Dorland et al.* [1997] and *Brasseur et al.* [1998a], based on a similar future scenario, suggest higher forcings of 0.28 W m^{-2} and 0.26 W m^{-2}, respectively. Model calculations have also been performed for other time horizons. *Roelofs et al.* [1998], for example, derived a forcing of 0.31 W m^{-2} for 2025, and *Stevenson et al.* [1998] derived a forcing of 0.19 W m^{-2} for 2100. These various studies, although performed under various assumptions regarding the future evolution of precursor emissions, suggest an increased contribution of ozone to the future anthropogenic radiative forcing of climate.

In this study, we use a newly developed CTM, called Model for Ozone and Related Chemical Tracers (MOZART), to investigate the evolution of tropospheric ozone from the preindustrial period to present and its potential evolution to the future under anthropogenic activities. The ozone changes are then introduced in a radiation model to derive the corresponding radiative forcing of climate. A comparison with ozone levels recorded at the surface during the nineteenth century is presented in order to provide some constraint on the background level of ozone in the troposphere. Sensitivity simulations are performed to investigate the role of various possible preindustrial ozone levels on the calculated forcing. The radiation code used in this study is similar to the one used by *Brasseur et al.* [1998a] and *Kiehl et al.* [1999] allowing for comparison with these previous estimates which used different ozone fields (from the IMAGES model and from observations, respectively). For the future scenario our simulation is only intended to provide an indication of the potential evolution and investigate the importance of tropical regions. The MOZART model is described in section 2. The changes in ozone and its precursors since the preindustrial period are presented in section 3.1, and the corresponding tropospheric ozone radiative forcing on climate is presented in section 3.2. Section 4 illustrates the potential changes in year 2050 as predicted by the model. The conclusions of this study are given in section 5.

2. Global Chemical-Tranport Model and Performed Simulations

The MOZART model is a three-dimensional chemical transport model of the global troposphere described and evaluated by *Brasseur et al.* [1998b] and *Hauglustaine et al.* [1998a]. This model has been developed in the framework of the National Center for Atmospheric Research (NCAR) Community Climate Model (CCM). In this version of MOZART (version 1) the time history of 56 chemical species is calculated on the global scale from the surface to the midstratosphere. The model accounts for surface emissions of chemical compounds (N_2O, CH_4, NMHCs, CO, NO_x, CH_2O, and acetone), advective transport (using the semi-Lagrangian transport scheme of *Williamson and Rasch* [1989]), convective transport (using the formulation of *Hack* [1994]), diffusive exchanges in the boundary layer (based on the parameterization of *Holtslag and Boville* [1993]), chemical and photochemical reactions, wet deposition of 11 soluble species, and surface dry deposition. The chemical scheme includes 140 chemical and photochemical reactions and considers the photochemical oxidation schemes of methane (CH_4), ethane (C_2H_6), propane (C_3H_8), ethylene (C_2H_4), propylene (C_3H_6), isoprene (C_5H_8), terpenes (α-pinene, $C_{10}H_{16}$), and a lumped compound n-butane (C_4H_{10}) used as a surrogate for heavier hydrocarbons. The evolution of species is calculated with a numerical time step of 20 min for both chemistry and transport processes. The model is run with a horizontal resolution which is identical to that of CCM (triangular truncation at 42 waves, T42) corresponding to about 2.8° in both latitude and longitude.

In the vertical the model uses hybrid sigma-pressure coordinates with 25 levels extending from the surface to the level of 3 mbar. Dynamical and other physical variables needed to calculate the resolved advective transport as well as smaller-scale exchanges and wet scavenging are precalculated by the NCAR CCM (version 2, Ω0.5 library) and provided every 3 hours from preestablished history tapes. Biomass burning emissions in MOZART account for fires in tropical and nontropical forests, savanna burning, fuel wood use, and agricultural waste burning. The spatial and temporal distributions of the amount of biomass burned is taken from *Hao and Liu* [1994] in the tropics and from *Müller* [1992] in nontropical regions. The emission ratios of each species relative to CO_2 are taken from *Granier et al.* [1996] for each type of biomass fire except for the CO and NO_x from savanna where the values suggested by *Hao et al.* [1996] and by *Andreae et al.* [1996], respectively, are considered.

A preliminary version of the model was used by *Brasseur et al.* [1996] to investigate the budget of chemical compounds in the Pacific troposphere in conjunction with the Mauna Loa Observatory Photochemistry Experiment (MLOPEX) measurements. More recent versions of the model were used by *Hauglustaine et al.* [1998b] in a study of ozone over the North Atlantic Ocean, by *Hauglustaine et al.* [1999] in a study of atmospheric composition changes associated with the 1997 Indonesian fires, by *Hauglustaine et al.* [2001] to investigate the role played by lightning NO_x emissions in the formation of tropospheric ozone plumes, and by *Emmons et al.* [1997, 2000] for a comparison of ozone and its precursors provided by various CTMs and data composites. With this version of MOZART we also participated in an intercomparison study of the modeled CO and O_3 global budgets [*Kanakidou et al.*, 1999a, 1999b], and in an intercomparison of model calculated and observed (during the Measurement of Ozone and Water Vapor by Airbus In-Service Aircraft, MOZAIC) ozone distributions in the upper troposphere [*Law et al.*, 2000].

Table 1 gives the global surface emissions used in MOZART for preindustrial, present-day, and future (2050) conditions. Present-day emissions are similar to those used by *Brasseur et al.* [1998b]. The only update to these emissions concerns the NO soil release based

Table 1. Preindustrial, Present-Day, and Future (2050) Global Emissions Used in MOZART[a]

Simulation	Industrial	Biomass Burning	Soils/Vegetation	Ocean	Total
		CO, Tg yr^{-1}			
Preindustrial	0.0	132.4	162.1	13.0	307.4
Present	381.6	661.8	162.1	13.0	1218.5
2050	721.6	731.3	162.1	13.0	1628.0
		NO_x, Tg N yr^{-1}			
Preindustrial	0.0	1.5	2.9	0.0	4.4
Present	21.4	7.5	4.7	0.0	33.6
2050	42.7	8.3	7.3	0.0	58.3
		CH_3COCH_3, Tg yr^{-1}			
Preindustrial	0.0	2.8	18.0	0.0	20.8
Present	1.5	14.0	18.0	0.0	33.5
2050	2.5	15.5	18.0	0.0	35.6
		CH_2O, Tg yr^{-1}			
Preindustrial	0.0	0.0	0.0	0.0	0.0
Present	2.3	0.0	0.0	0.0	2.3
2050	3.9	0.0	0.0	0.0	3.9
		NMHCs, Tg C yr^{-1}			
Preindustrial	0.0	7.5	80.7	78.5	166.7
Present	79.5	37.6	80.7	78.5	276.3
2050	177.2	41.4	80.7	78.5	377.8
Isoprene, Tg C yr^{-1}	0.0	0.0	220.0	0.0	220.0
Terpenes, Tg C yr^{-1}	0.0	0.0	129.5	0.0	129.5

[a]Lightning NO_x emissions are fixed to 7 Tg N in MOZART for both preindustrial, present-day, and future conditions. Aircraft NO_x emissions are 0 for preindustrial, 0.51 Tg N for present-day, and 1.69 Tg N in 2050 [*IPCC*, 1999].

on *Yienger and Levy* [1995] which totals 4.7 Tg N yr^{-1} instead of the 6.6 Tg N yr^{-1} used in the earlier version of MOZART and based on *Müller* [1992]. For the preindustrial simulation the industrial emissions are set to zero. There is a high uncertainty on preindustrial biomass burning emissions. Owing to the lack of information, we make the simple assumption that the preindustrial emissions were only 20% of their present-day global value, with similar geographical and seasonal distributions. Previous modeling studies have used similar assumptions, and reduced their global biomass burning emissions to 10–25% of their present estimate [e.g., *Wang and Jacob*, 1998; *Berntsen et al.*, 1997; *Roelofs et al.*, 1997]. These decreased emissions account for lower population in the tropics at that period. It should be noted, however, that changes in the emission patterns of emissions have also occured. Here again, little information is available even though it is believed that deforestation has been more affected than savanna burning or boreal forest fires. These geographical differences are not considered in this study. An extreme case, with biomass burning emissions completely shut off, has also been considered to put some bounds to the problem, simulated and will be discussed below. Natural (i.e., vegetation, soils, and ocean) emissions are unchanged for all simulations. For NO soil emissions, as described by *Yienger and Levy* [1995], the emissions are modified to account for fertilizer use in relation to changing agricultural activities. The natural soil emissions calculated with the model of *Yienger and Levy* [1995] total 2.9 Tg N yr^{-1}, corresponding to about 60% of the present-day value of all soil emissions. Plate 1 shows the annual NO soil emissions calculated by *Yienger and Levy* [1995] and used for the MOZART preindustrial and present-day simulations. The change in the geographical distribution from the preindustrial to present occurs primarily through enhanced emissions in northern America, Europe, China, and India due to the application of fertilizer in these regions. As will be discussed later, this feature is particularly important when calculating preindustrial ozone, as soil emissions were the major surface source of NO_x around 1850.

Future emission estimates are based on the IPCC reference scenario IS92a [*IPCC*, 1992]. The assumptions, methodology, and results of the various 1992 IPCC scenarios (IS92a through f) have been summarized by *IPCC* [1992] and are described in more detail by *Pepper et al.* [1992]. New scenarios (SRES) have recently been proposed [*IPCC*, 2000] for the IPCC third assessment report. A preliminary version of the SRES scenarios has been used recently by *Stevenson et al.* [2000]. In this study, however, we use the 1992 scenarios since they have been used in several other modeling studies and can be regarded as a reference case for model intercomparisons. IS92a is considered here as a business-as-usual scenario with moderated abatement measures and is used for reference. New simulations using the new SRES scenarios will be reported elsewhere. We consider in this study a time horizon of 50 years and present the results for year 2050. Assumptions on population and economic growth are key drivers of energy use and overall industrial activity. These evolutions are expected to vary significantly from one region to another in the future. Therefore not only the global emissions have been modified but also their geographical distribution. This feature is of particular importance regarding the photochemistry of ozone. The global emissions, as adopted in the model, are modified according to scaling factors provided for the different chemical species and emission types according to IS92a. As reported by *Pepper et al.* [1992], these scaling factors are modified on the basis of four regions: OECD countries, Russia/Eastern Europe, China/Centrally Planned Asia, and other countries. Table 1 provides the resulting global emissions obtained for 2050, and Plate 2 illustrates the geographical distributions of total CO and NO_x emissions for both present-day and 2050 conditions. This plate clearly shows the increase in surface emissions in Southeast Asia, India, and Central America as a consequence of growing industrial activities. To a lesser extent, increased emissions are also predicted in Africa and South America, mainly as a consequence of enhanced biomass burning emissions. In the northern hemisphere, emissions over the United States and Europe are slightly reduced due to the moderated abatement measures assumed in the IS92a scenario.

In MOZART, as described by *Brasseur et al.* [1998b], the distribution of several long-lived species (O_3, NO_x, HNO_3, N_2O_5, CO, CH_4, and N_2O) are prescribed above 60 mbar (or approximately 20 km altitude), according to monthly and zonally averaged values provided by the middle atmosphere 3-D STARS model [*Brasseur et al.*, 1997]. For all simulations the distributions of O_3, NO_x, HNO_3, N_2O_5, and CO are unchanged above this altitude. However, in the lower stratosphere, the distribution of these species can be affected by photochemistry and transport. Note that version 1 of MOZART does not account for chlorine and bromine chemistry in the stratosphere. Because of their long lifetime compared to the model integration time (i.e., 2 years), CH_4 and N_2O concentrations are scaled in the troposphere to their concentrations determined from ice core analyses for the preindustrial simulation and to their 2050 global concentrations as provided by *IPCC* [1992] for the future simulation.

In order to investigate the contribution of the stratospheric influx to the calculated ozone levels in the troposphere, a stratospheric ozone-like tracer is added in MOZART. As described by *Hauglustaine et al.* [2001], this tracer is imposed to be identical to the modeled real ozone above the model tropopause. Below the tropopause the photochemical production is set equal to zero, while a photochemical loss is attributed to ozone photolysis followed by the reaction of $O(^1D)$ with water

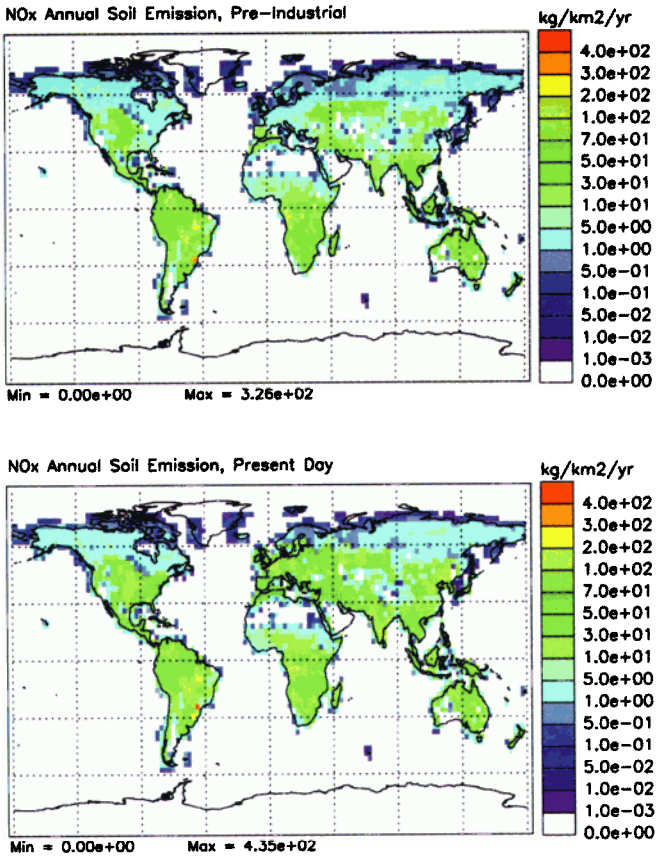

Plate 1. Annual NO soil emissions calculated with the model of *Yienger and Levy* [1995] for preindustrial and present-day conditions (kg N km^{-2} yr^{-1}).

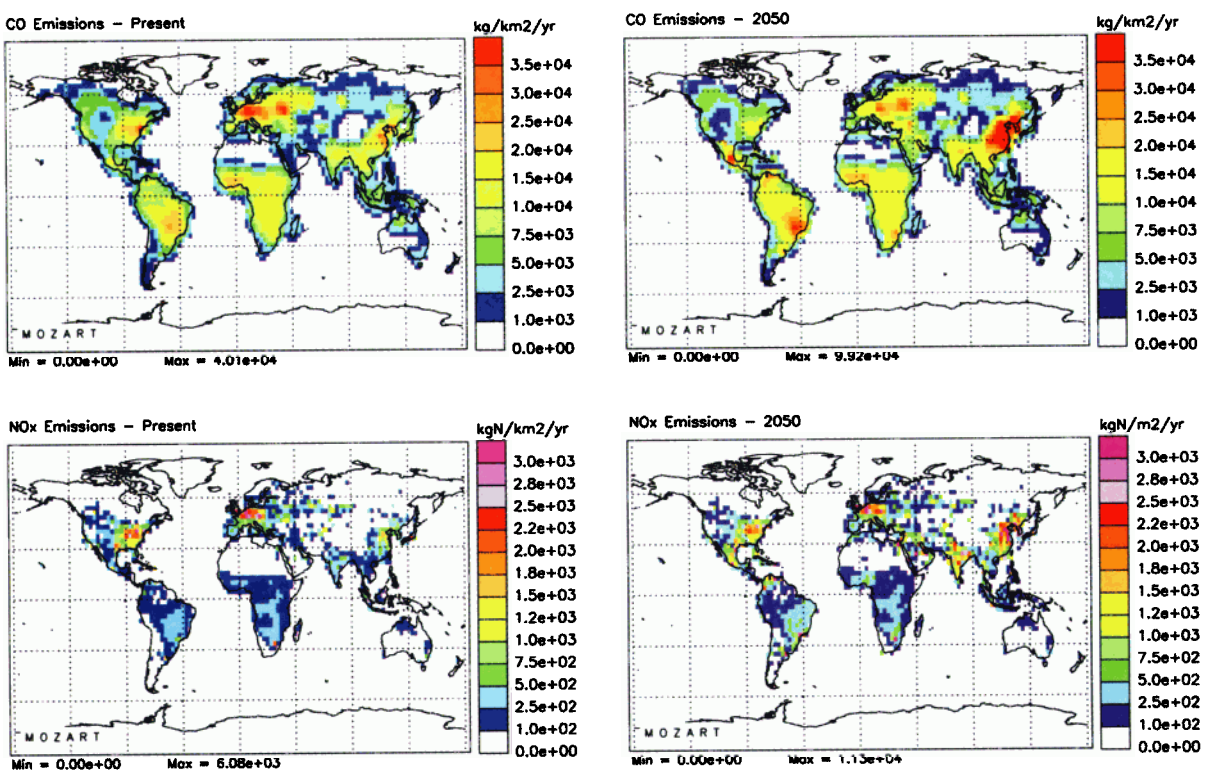

Plate 2. Present and future (2050) annual surface emissions of CO (kg km^{-2} yr^{-1}) and NO_x (kg N km^{-2} yr^{-1}).

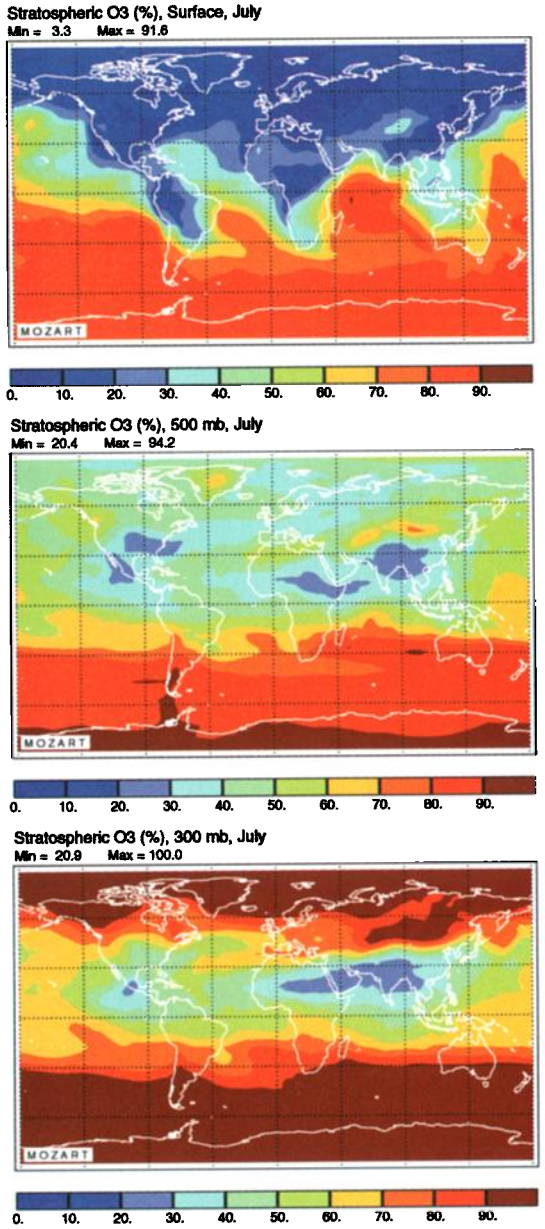

Plate 3. Contribution of stratospheric ozone to the ozone distribution at the surface, 500 mbar, and 300 mbar calculated for July conditions (percent).

vapor, to reaction of ozone with OH and HO_2, and to reaction of ozone with NMHCs. Dry deposition at the surface is also considered for this so-called stratospheric ozone tracer. A similar definition for a stratospheric ozone tracer has been used by *Roelofs and Lelieveld* [1997].

The contribution of the ozone influx from the stratosphere to the calculated tropospheric ozone levels is calculated as the ratio between the stratospheric tracer and the modeled real ozone. This ratio, expressed in percent, is illustrated for present-day conditions on Plate 3 for July conditions for three different altitude levels. Over the continents in the northern hemisphere, the stratospheric contribution is minimum in the boundary layer (only a few percent) as, near the surface, ozone is almost entirely photochemically produced from the release of its precursors by industrial and natural emissions. Similarly, minimum stratospheric contributions are calculated in the tropics (e.g., South America, Africa) where photochemical production from biomass burning and biogenic emissions of precursors prevails. The photochemical influence is also clear in the midtroposphere (500 mbar) over most of the northern hemisphere, where the stratospheric contribution represents 20-30% of the ozone level over polluted regions and 30-50% over oceanic regions. In the southern hemisphere extratropics, however, the influence of stratospheric input is dominant during this season and generally higher than 80% at all altitudes. Meridional transport of ozone originating from the stratosphere to the tropics, into the South Pacific, South Atlantic, and Indian Oceans is simulated with this model. At 300 mbar, high and midlatitudes are located within the stratosphere. However, the contribution of photochemical production in the troposphere is still high in the tropics where strong upward transport and convection prevail. The stratospheric tracer will be used in the following sections to provide a lower limit on preindustrial ozone background levels.

3. Evolution of Tropospheric Ozone and Its Precursors Since the Preindustrial Era

3.1. Changes in Atmospheric Composition

For present-day conditions the calculated surface NO_x mixing ratio reaches more than 5 ppbv over Europe, eastern Asia, and North America. These high values are due primarily to fossil fuel emissions (Plate 4). In the biomass burning regions of Africa and South America the calculated mixing ratio is typically in the range 1-3 ppbv. As illustrated by Plate 4, preindustrial levels are significantly lower over source regions. Over the continents, biogenic soil emission is the main preindustrial surface source of NO_x. The NO_x patterns follow the distribution of soil emissions with background values lower than 40 pptv and maximum values of typically 300-500 pptv at northern midlatitudes where soil emissions are high. The calculated preindustrial distribution of NO_x is less uniform in space than reported by *Berntsen et al.* [1997]. These authors estimated mixing ratios generally larger than 100 pptv in the boundary layer. In the tropics the simulated preindustrial levels reach locally 500-1000 pptv due to maximum biogenic emissions in these regions (see Plate 2) and residual biomass burning emissions. We find the preindustrial NO_x distribution in the boundary layer to be controlled primarily by natural soil emissions at northern midlatitudes and therefore very sensitive to assumptions made for these emissions. It is therefore crucial to determine the natural soil emissions in the absence of nitrogen release by

fertilizers [*Yienger and Levy*, 1995]. Uncertainties in estimating natural NO_x from soils and from lightning will strongly affect the calculated preindustrial ozone concentrations. A similar conclusion was reached by *Lelieveld and Dentener* [2000] for their 1860 simulation.

The calculated preindustrial and present-day CO distributions at the surface are shown on Plate 4 for July conditions. Present-day values reach more than 200 ppbv in polluted regions in the northern hemisphere and in the tropics over biomass burning regions. An interhemispheric difference of more than 50 ppbv is calculated with values of 100-150 ppbv north of about 50°N and background mixing ratios of 50-70 ppbv over the ocean in the southern hemisphere. Preindustrial mixing ratios are significantly lower with background levels in the range 20-40 ppbv in oceanic regions. Over the continents, mixing ratios of 40-60 ppbv are predicted and mainly associated with CO biogenic emissions (soils) and production of CO through oxidation of biogenic hydrocarbons (i.e., isoprene and terpenes). In the tropics, due to important biogenic hydrocarbon emissions and residual biomass burning, maximum values of 60-80 ppbv are calculated.

Preindustrial CO levels have been estimated from ice cores in Antarctica (50-60 ppbv) and Greenland (90 ppbv) by *Haan et al.* [1996] and *Haan and Raynaud* [1998]. These studies suggest that carbon monoxide did not change significantly during the last 150 years in polar regions. Our calculated preindustrial CO levels sampled over a full annual cycle over Antarctica and Greenland are in the range 19-22 ppbv and 35-55 ppbv, respectively. These results are at odds with the ice core analyses. A similar disagreement has also been reached by other models [*Wang and Jacob*, 1998]. The Antarctic levels measured by *Haan et al.* [1996] are also inconsistent with the lower preindustrial methane abundance. Possible contamination of the ice sample during the experimental procedure is, however, not excluded (J. Chappellaz, personal communication, 2000), and the polar ice core measurements are currently being reexamined.

The CO global budget given in Table 2 indicates that the preindustrial CO burden, as calculated by MOZART, is 3 times lower than the current value, reflecting lower direct surface emissions and a reduced photochemical production through CH_4 and NMHCs oxidation. More abundant OH concentrations at preindustrial times also contribute to lower CO densities. A 16 day increase in the CO photochemical lifetime (from 1.4 to 2 months) is calculated from preindustrial to present. Similarly, the methane lifetime estimated by the model increases from 7 years at preindustrial times to 9.3 years for present-day conditions. These changes in lifetime reflect the strong impact of human activities on the oxidizing capacity of the atmosphere, with a global decrease of OH by 33% in the last 150 years.

The simulated preindustrial and present-day ozone surface mixing ratios are illustrated on Plate 5 for January and July conditions. The preindustrial levels over the continents in the northern hemisphere range from a minimum value of 5-15 ppbv in January, associated with chemical loss and dry deposition, to a summer value reaching 10 ppbv in Europe and 20 ppbv in the central United States where NO soil emissions and, consequently, NO_x preindustrial levels are at maximum (see Plate 4). In the southern hemisphere the preindustrial mixing ratios over the ocean ranges from only 4-8 ppbv in January due to chemical loss to values of 10-20 ppbv in July associated with a seasonal maximum of influx from the stratosphere (see Plate 3). The present-day distributions clearly emphasize a strong impact of anthropogenic activities on ozone levels at a global scale. Maximum O_3 mixing ratios reaching 50-60 ppbv are calculated over polluted regions (i.e., northern America, Europe, and Southeast Asia) during summer in the northern hemisphere. Export of ozone rich air from the United States and from Europe to the northern Atlantic is visible in July, with ozone mixing ratios reaching 25-30 ppbv in the export plumes over the ocean. The background ozone levels calculated over the ocean in the southern hemisphere have increased by 5-10 ppbv in comparison to preindustrial values.

Table 2. Annual Budget of Carbon Monoxide in the Troposphere (Below 250 mbar) Calculated by MOZART for Preindustrial, Present-Day, and Future (2050) Conditions, and Atmospheric Lifetime of CO and CH_4[a]

	Preindustrial	Present Day	2050
Surface emission	307	1218	1628
Photochemical production	596	1004	1334
Photochemical destruction	−768	−1856	−2454
Dry deposition	−59	−184	−251
Burden, Tg CO	92	305	440
CO lifetime, month	1.44	1.97	2.15
CH_4 lifetime, years	6.97	9.28	10.21

[a]Units are in Tg CO yr^{-1}.

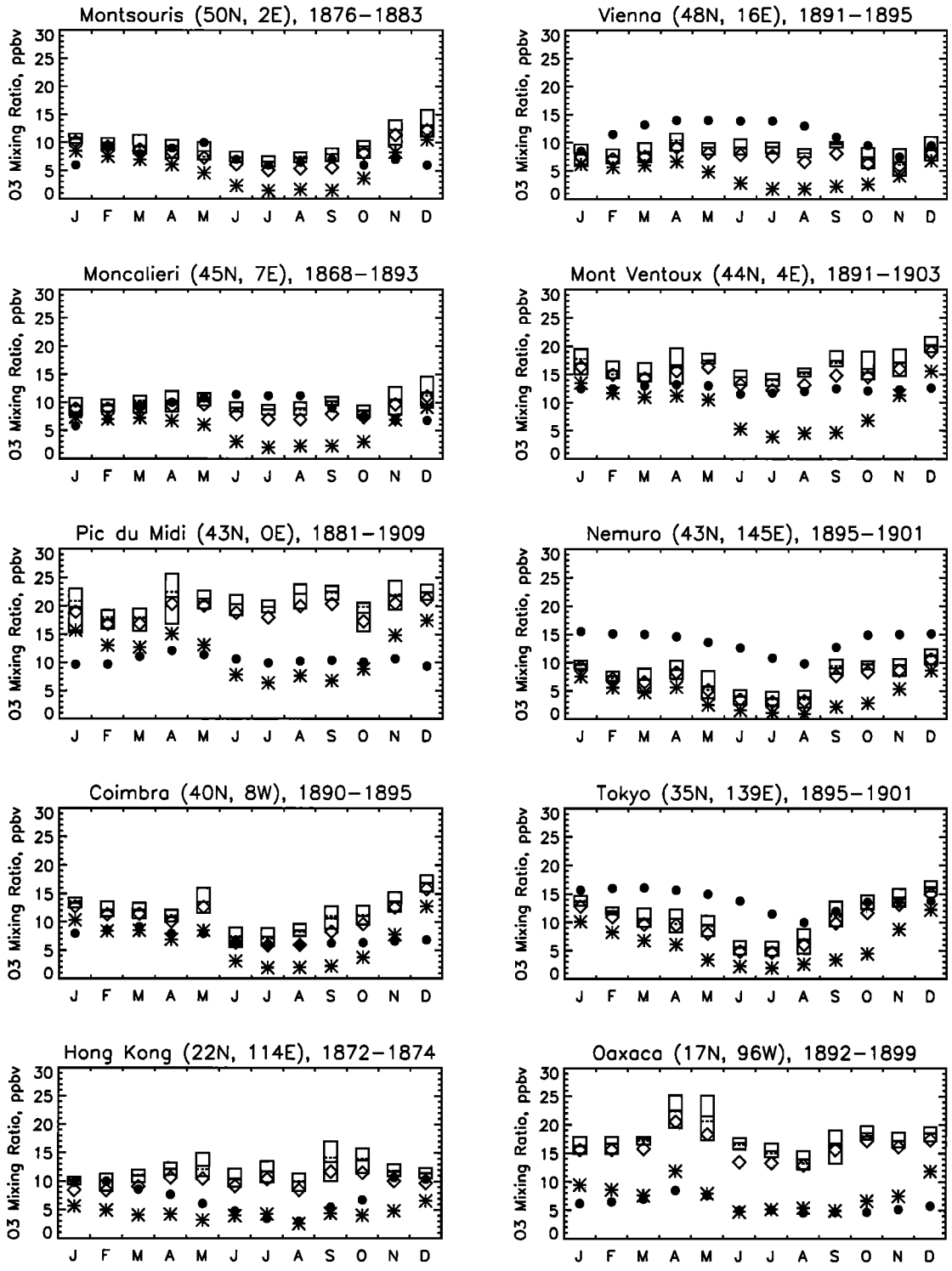

Figure 1. Seasonal cycle of surface ozone for the preindustrial period (ppbv). Dots, measurements (see text for details); box-wisker plot, model monthly mean and standard deviation; stars, stratospheric ozone contribution; open diamonds, calculated ozone neglecting biomass burning emissions.

Surface ozone levels recorded during the nineteenth century have been re-evaluated in the literature and reported at various sites [see, e.g., *Marenco et al.*, 1994]. These historical measurements in ambient air were made using the Schönbein paper method. This technique is not strictly quantitative and suffers from interference from various sources. In particular, relative humidity, temperature, and also wind speed can affect the ozone reading. Other pollutants can also increase (e.g., H_2O_2, HO_2, NO_2, PAN), or decrease (SO_2, NH_3) the ozone reading. For these reasons, the possibility of deriving reliable information on past ozone levels from the

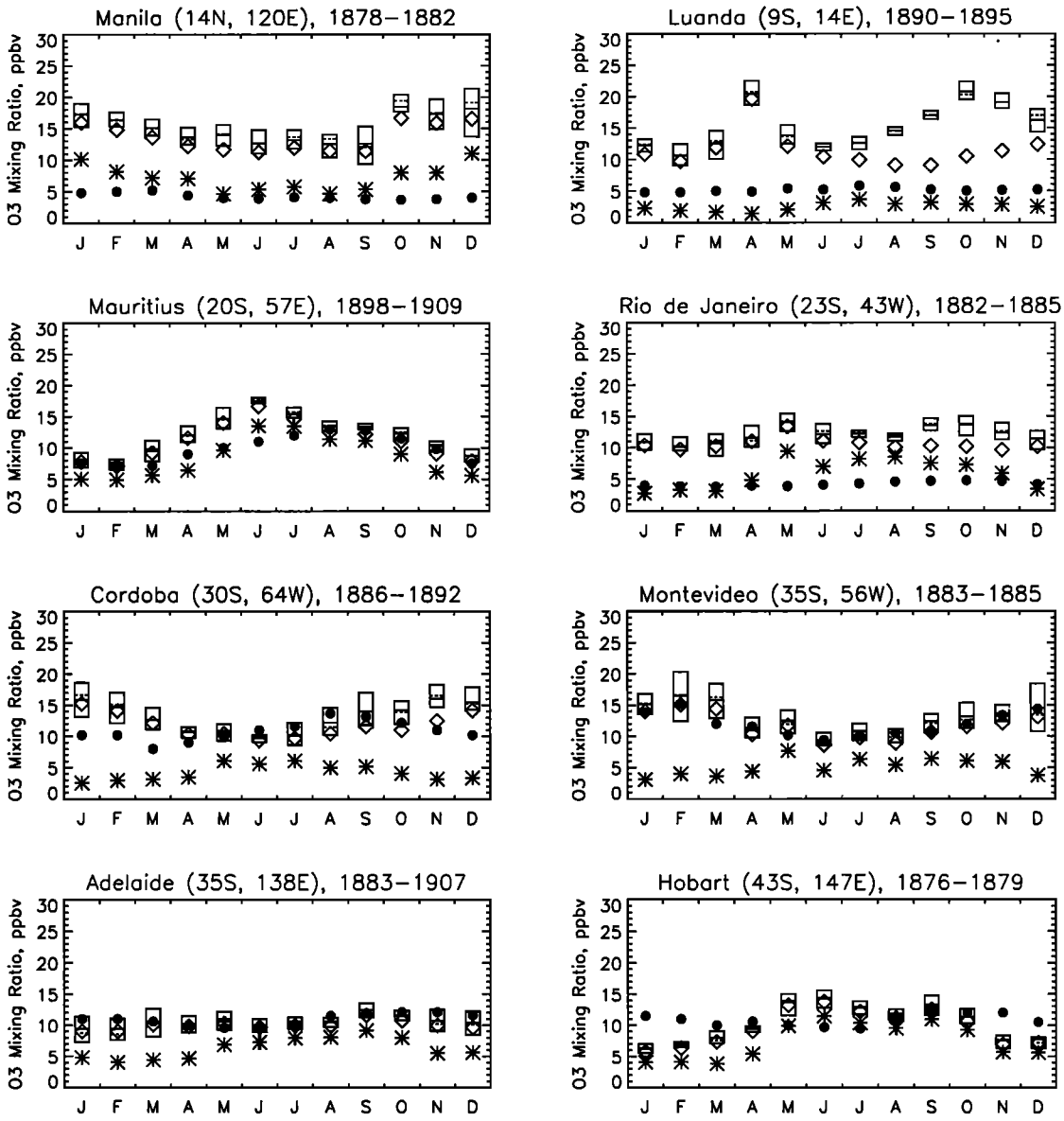

Figure 1. (continued)

Schönbein technique is controversial. However, several authors have used proper correction techniques and calibration procedures to reassess these historical levels and derive useful information. Bearing these limitations in mind, in this study we compare the measurements to the model results to provide some constraint on our calculations. The nineteenth century ozone levels considered here are taken from *Volz and Kley* [1988] for Montsouris (France), *Anfossi et al.* [1991] for Moncalieri (Italy), *Sandroni et al.* [1992] for Montevideo (Uruguay), and Cordoba (Argentina), and *Marenco et al.* [1994] for the Pic du Midi (southwestern France). Historical data at Manila (Philippines), Rio de Janeiro (Brazil), and Oaxaca de Juarez (Mexico) are taken from *Sandroni and Anfossi* [1994]. Measurements reported at Vienna (Austria), Mont Ventoux (France), Nemuro and Tokyo (Japan), Coimbra (Portugal), Hong Kong, Luanda (Angola), Mauritius, Adelaide (Australia), and Hobart (Tasmania) are taken from *Pavelin et al.* [1999].

The preindustrial ozone mixing ratios calculated with MOZART at the historical sites are compared to the measurements on Figure 1. As noted by *Pavelin et al.* [1999], the error bar on the observed value is large (±5 ppbv or larger). The stratospheric ozone tracer (see section 2) at the location is also shown for comparison. We find a fairly good agreement between model and measurements at several extratropical and midlatitude stations previously used for model evaluation. This is particularly the case for the European stations of Montsouris, Moncalieri, and in the southern hemisphere at Montevideo and Adelaide. At these stations, fairly constant mixing ratios of 5-10 ppbv are obtained throughout the year. This is clearly in contrast with typical seasonal cycles simulated for present-day conditions exhibiting maximum mixing ratios associated with photochemical production during sum-

mer [*Hauglustaine et al.*, 1998a]. During winter and spring, comparisons with the stratospheric tracer show that ozone is mainly from stratospheric origin. During summer an ozone enhancement of about 5 ppbv is calculated and associated with biogenic emissions of precursors. At the two southern hemisphere stations of Cordoba and, to a lesser extent, Hobart, a fairly good agreement is reached except during the summer period. A fairly good agreement is also obtained at the altitude site of Mont Ventoux (1910 m). However, during winter and spring, an overestimate of 5-10 ppbv points toward an excess contribution from stratospheric input in the model. At this site the stratospheric tracer clearly shows a large contribution of the stratospheric influx from November to May. A different picture is obtained at the second altitude site of Pic du Midi (2860 m), where a ozone is systematically overestimated by 10-15 ppbv. A similar disagreement has been obtained at this site by *Wang and Jacob* [1998]. During winter and spring the contribution of stratospheric ozone at this altitude is even larger than the measurements by 5-8 ppbv. This feature would point toward an overestimate of stratospheric influx in MOZART. During summer a tropospheric ozone excess is simulated. Absence of dry deposition in the model at this altitude (associated with a too coarse resolution to properly account for the Pyrenees mountains) would also be a possible explanation for the disagreement. However, according to *Marenco et al.* [1994], the Pic du Midi data are representative of free tropospheric air. A systematic disagreement is obtained in the tropics at continental stations. At Oaxaca, Manila, Luanda, and Rio the measurements seem to provide mixing ratios close to 5 ppbv and even less, while the modeled values are in the range 10-15 ppbv or even as high as 20 ppbv. In order to investigate the potential role played by the residual biomass burning emissions (20% of present-day value), a preindustrial case, in which biomass burning emissions are omitted, has been performed. As shown by Figure 1, even in this extreme case, the calculated mixing ratios still overestimate the measurements by 10-15 ppbv in the tropics. For the station of Luanda the comparison has, however, improved during August-November. For the stations of Vienna, Nemuro, and Tokyo, measured values are larger than model results regardless of the season. The reasons for this disagreement are not clear. A relatively good agreement is reached with this model at midlatitude locations. This contrasts with the systematic overestimate reported by previous studies [*Berntsen et al.*, 1997; *Wang and Jacob*, 1998; *Mickley et al.*, 2001]. The calculated preindustrial ozone levels at these altitudes are found to be particularly sensitive to the NO soil emissions used in the model. Natural soil emissions appear crucial for the simulation of surface ozone for pristine conditions. In the tropics a systematic overestimate is reached with this model. We note, however, that the observed levels of only 5 ppbv are surprisingly low and possibly reflect problems with the ozone reading from the Schönbein paper. Again, we would like to stress the large error bar associated with the historical data. Disagreement (or agreement) noted in Figure 1 may well be insignificant.

The modeled relative ozone change since preindustrial times (present to preindustrial ozone ratio) indicates a general increase of surface levels by more than a factor of 2 during July in the northern hemisphere when photochemical production is a maximum (Plate 6). The ozone concentration increase reaches more than a factor of 5 over polluted regions. Export of ozone (increase by a factor of 3-4) to the northern Atlantic and to northern polar latitudes is also visible. In January, ozone increases roughly by 50-80% over the ocean in the northern hemisphere and by a factor of 2- 3 over the continents. Over the ocean in the southern hemisphere the O_3 concentration increases by only 10-20% in July (when transport from the stratosphere dominates) and by 30-50% in January. The ozone increase associated with biomass burning is also visible in the tropics with local increases reaching a factor of 2-3. The ozone increase is also visible in the midtroposphere (500 mbar) in the northern hemisphere. In July, export of ozone from polluted regions is responsible for a general increase reaching a factor of 2-3. A similar relative ozone increase has also been reported by *Levy et al.* [1997]. In the tropics and subtropics, due to vigorous upward transport, the ozone density increases by 70-100% up to 200 mbar where the impact on climate is the largest [*Lacis et al.*, 1990; *Hauglustaine and Granier*, 1995].

Plate 7 provides a different perspective on the ozone change as a function of altitude, and shows the increase in the zonal mean distribution of ozone for January and July conditions. As shown earlier, the maximum ozone increase is found at midlatitudes in the northern hemisphere during July and reaches a factor of 3 at the surface. Transport from the polluted boundary layer to the mid and upper troposphere is visible. In particular, in both seasons a secondary maximum reaching more than 50% is calculated in the tropical upper troposphere. The ozone change is in line with the results presented by *Berntsen et al.* [1997] and *Stevenson et al.* [1998] with calculated ozone increases in the upper troposphere reaching 15 ppbv and 30 ppbv, respectively, in the northern hemisphere during January and July, and 15-20 ppbv in the tropics. At the surface, ozone increases by 25-30 ppbv at northern midlatitudes and by less than 10 ppbv in the southern hemisphere.

In most of these previous studies the ozone influx from the stratosphere remained unchanged between preindustrial and present-day conditions [*Wang and Jacob*, 1998; *Stevenson et al.*, 1998; *Mickley et al.*, 1999]. In other cases the ozone mixing ratios in the stratosphere were held constant [*Brasseur et al.*, 1998a; *Berntsen et al.*, 1997; *Roelofs et al.*, 1997]. In MOZART the increase in tropospheric ozone concentration and subsequent transport through the tropopause is responsible for an increase in the lower stratosphere in all seasons.

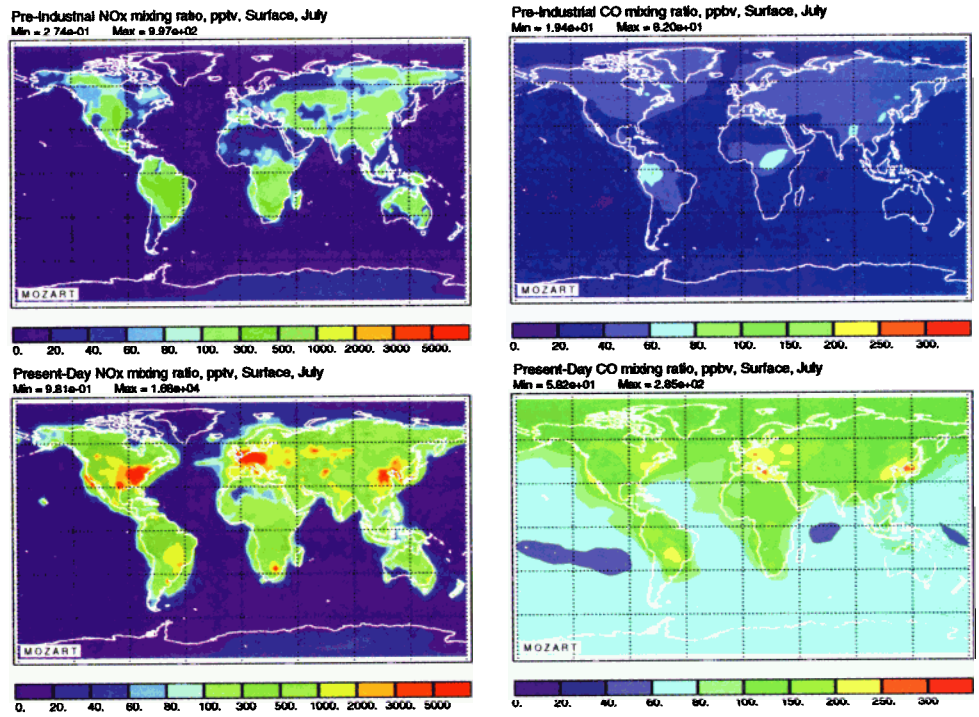

Plate 4. (left) Surface distribution of NO_x calculated in July for preindustrial and present-day conditions (pptv). (right) Surface distribution of CO calculated in July for preindustrial and present-day conditions (ppbv).

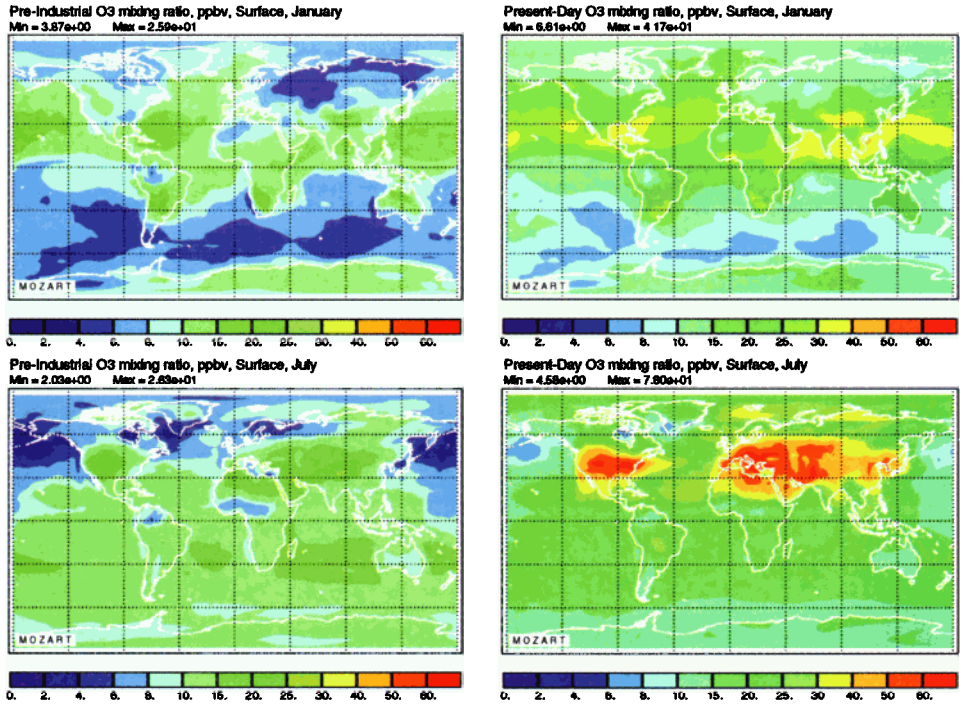

Plate 5. Surface distribution of O_3 calculated in January and July for preindustrial and present-day conditions (ppbv).

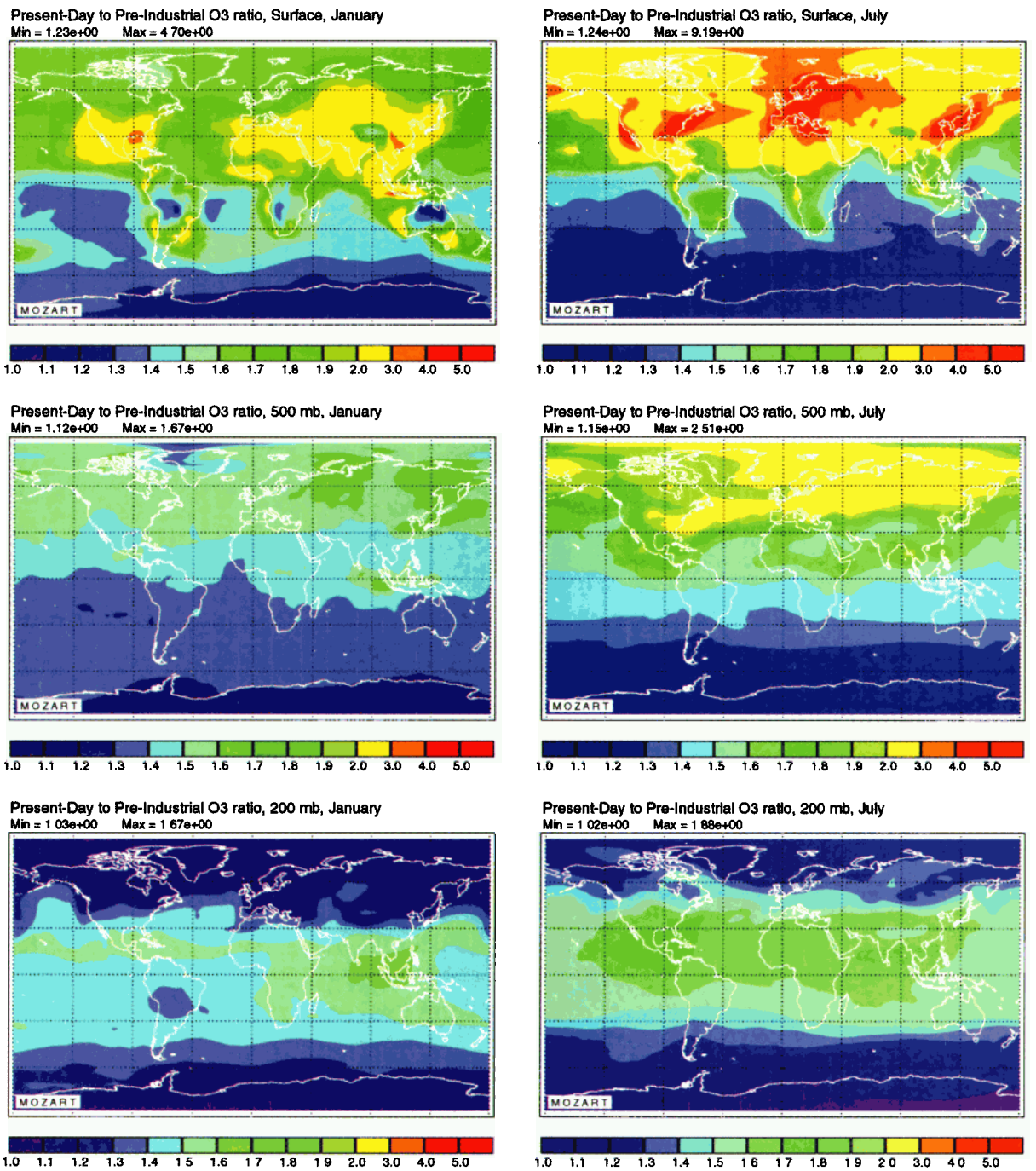

Plate 6. Relative ozone increase from pre-indutrial to present calculated at the surface, 500 mbar, and 200 mbar for January and July conditions.

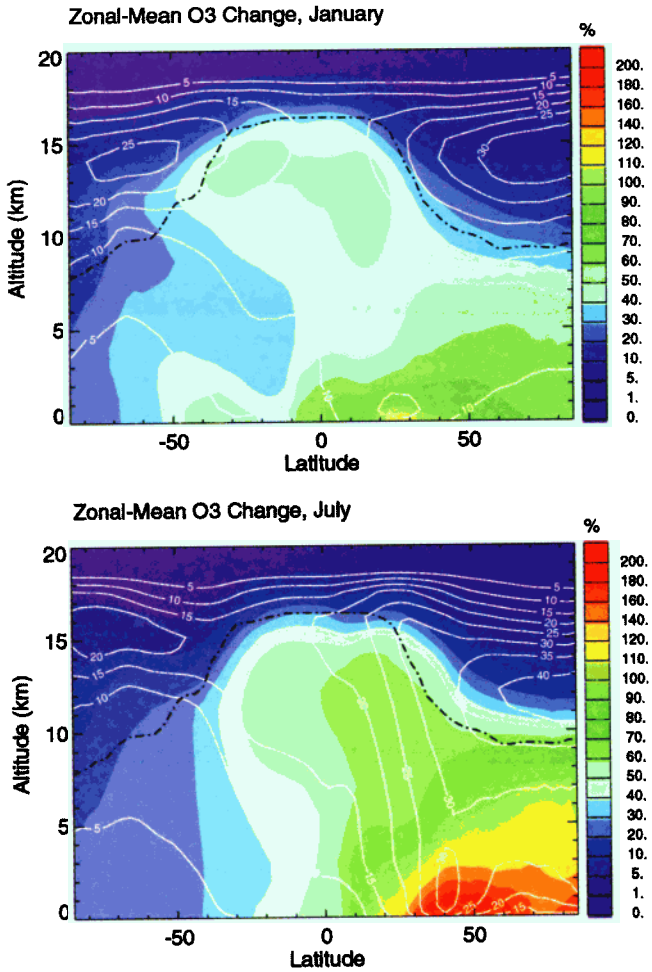

Plate 7. Zonal mean change in ozone from preindutrial to present for January and July conditions. Shaded contours give the change in percent, and solid contours give the increase in ppbv.

These maxima reach 20-40 ppbv in absolute values (less than 10-20%). A similar conclusion has been reached by *Lelieveld and Dentener* [2000]. It should be noted that the actual version of the MOZART model does not include chlorine and bromine chemistry in the stratosphere. Therefore, in the present study, we focus on tropospheric ozone changes only and do not consider the impact of stratospheric ozone changes on the chemistry of the troposphere. As illustrated by *Kiehl et al.* [1999], the zonal and annual mean ozone concentration in the lower stratosphere at high latitudes has decreased by typically 10–20% due to stratospheric ozone catalytical destruction.

Plate 8 shows the change in the tropospheric ozone column for January and July, and Figure 2 shows the corresponding seasonal evolution as a function of latitude. We adopt here a thermal definition of the tropopause as the lowest model level at which the temperature vertical gradient decreases below 2 K km^{-1}. The resulting tropopause height, illustrated on Plate 7, ranges from 8 km in polar regions to 16 km in the tropics, in agreement with more sophisticated definitions [see, e.g., *Hoinka*, 1998]. The resulting change in the tropospheric column reaches maximum values of 30-40 Dobson units (DU) (20 DU in zonal mean) over the polluted regions (40°-50°N) of the northern hemisphere in July. A strong export of ozone to polar regions is simulated by the model and results in an ozone increase reaching 16-18 DU in zonal mean at northern polar latitudes during summer. In January a more uniform increase of 10 DU or less is calculated in the southern hemisphere, and a column increase of 8-12 DU is calculated in the northern hemisphere. In the tropics an ozone increase associated with a peak in biomass burning activity reaching 8-10 DU in zonal mean is predicted in October (10°-20°S). The seasonal and geographical distributions of the tropospheric ozone column increase are in good agreement with the previous estimate by *Kiehl et al.* [1999]. In particular, a similar maximum is predicted at mid and high latitudes during summer in the northern hemisphere and in the tropics during the peak in biomass burning activity (i.e., September-October). We note, however, that the amplitude of the maximum is larger in the previous study by about 2-8 DU in comparison to our estimate. Different preindustrial levels are a possible source of discrepancy with this previous work.

Table 3 provides the calculated tropospheric ozone budgets (up to 250 mbar) for preindustrial and present-day conditions. The impact of anthropogenic activities on ozone photochemical production induces an 85% in-

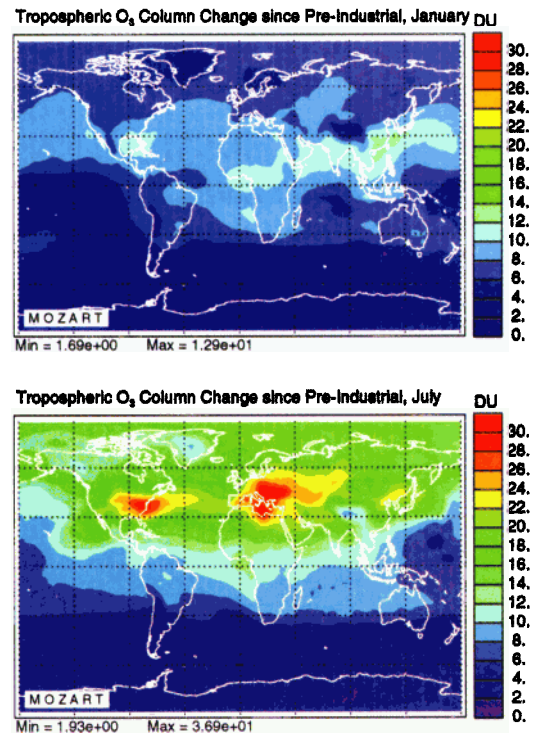

Plate 8. Tropospheric ozone column increase from preindutrial to present calculated for January and July conditions (DU).

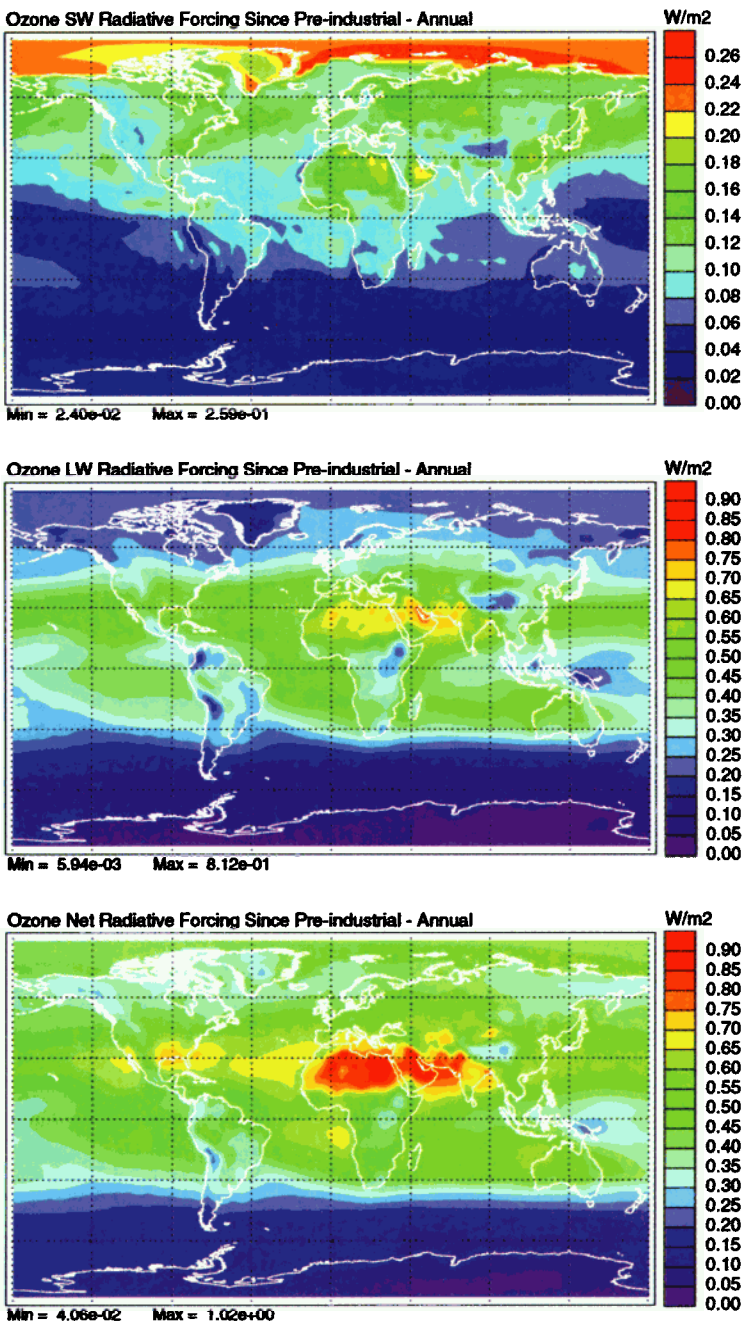

Plate 9. Annual mean tropospheric ozone radiative forcing at the tropopause calculated from pre-indutrial to present (W m^{-2}). (top) Shortwave forcing, (middle) longwave forcing, and (bottom) total forcing (shortwave plus longwave). Note the different color scale of the SW forcing.

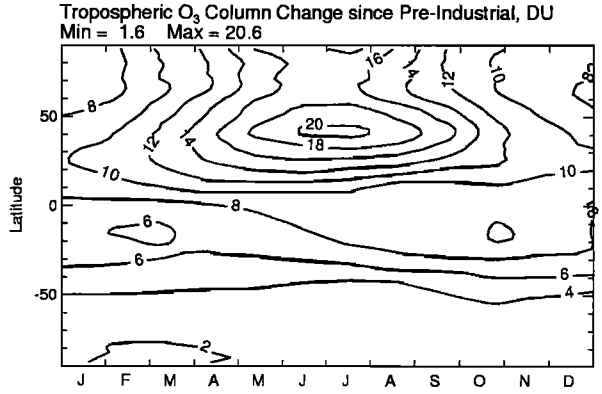

Figure 2. Seasonal cycle of calculated zonal-mean tropospheric ozone column change since the preindustrial period (DU).

crease (+1686 Tg) since the preindustrial era. The photochemical loss and dry deposition at the surface increase by 60% (+1026 Tg) and by about 100% (+686 Tg), respectively. As a consequence of this increase in ozone loss processes, the global lifetime of ozone decreases from about 20.5 to 18.6 days. Since the influx from the stratosphere is not fixed in MOZART, we calculate a small increase (7% or 27 Tg) of this term associated with the enhanced ozone concentration in the lower stratosphere and its subsequent intrusion into the troposphere. For both preindustrial and present conditions the ozone budget is characterized by a global net photochemical production. This term increases by about a factor of 2 over the last 150 years. The global tropospheric ozone content increases by about 57% (+75 Tg) as a consequence of increased emissions in precursors.

3.2. Tropospheric Ozone Radiative Forcing of Climate

The tropospheric ozone changes calculated by the MOZART model have been used to derive the associated radiative forcing of climate. The forcings are calculated with a modified version of the NCAR CCM3 radiation model as described by *Kiehl et al.* [1998, 1999]. The temperature, water vapor, and cloud properties and distributions are obtained from the NCAR CCM. In the longwave part of the spectrum the model employs a broadband scheme which does not include the effects of the weak 14 micron band of ozone [*Shine et al.*, 1995]. In the troposphere the pressure broadening reduces the contribution of this 14 micron band to about 2%. The shortwave model is based on a δ-Eddington scheme using 18 intervals [*Briegleb*, 1992]. The horizontal resolution of the radiation model is similar to that of MOZART (i.e., 2.8° by 2.8°) with the standard 19 levels of the CCM in the vertical. The shortwave and longwave radiative forcings are calculated at the tropopause. As indicated earlier, the tropopause is defined as the lowest model level at which the temperature vertical gradient decreases below 2 K km^{-1}. Above this level the stratospheric temperature is adjusted according to the Fixed Dynamical Heating (FDH) approximation [*Ramanathan and Dickinson*, 1979]. The thermodynamic equation is integrated in the stratosphere until a convergence of 0.001 K is reached at all levels. Only the ozone change calculated in the troposphere is considered for radiative forcing calculations. Above the tropopause the ozone perturbation is not accounted for.

Plate 9 shows the geographical distribution of the annual mean forcings (shortwave, longwave, and total) associated with tropospheric ozone increase since the preindustrial period. The forcing has been calculated for total (clear and cloudy) sky conditions. The shortwave (SW) forcing reaches a maximum of 0.26 W m^{-2} in northern polar regions. This maximum is associated with ozone transport from polluted regions to the Arctic as shown by Plate 8, and to increased absorption of solar radiation above a high-albedo surface. A secondary maximum in SW forcing is also predicted over the Sahara where the surface albedo is high. The globally averaged SW forcing is 0.09 W m^{-2} (see Table 4). The longwave (LW) forcing reaches maximum values of 0.7–0.8 W m^{-2} in the tropics and subtropics where the temperature difference between the surface and the tropopause is the largest. A high forcing reaching 0.6 W m^{-2} is calculated over the South Atlantic and is associated with biomass burning emissions. The calculated global mean LW forcing is 0.34 W m^{-2}. The total

Table 3. Annual Budget of Ozone in the Troposphere (Below 250 mbar) Calculated by MOZART for Preindustrial, Present-Day, and Future Conditions[a]

	Preindustrial	Present Day	2050
Photochemical production	1989	3675	4661
Stratospheric influx	364	391	395
Photochemical destruction	−1681	−2707	−3338
Dry deposition	−672	−1358	−1718
Net chemistry	308	968	1323
Burden, Tg	132	207	253
O_3 lifetime, days	20.5	18.6	18.3

[a]Units are in Tg O_3 yr^{-1}.

Table 4. Global Mean Radiative Forcings Associated With Tropospheric Ozone Increase[a]

	DU	LW	SW	Total	Normalized
		Preindustrial to Present			
Clear sky	8.9	0.45	0.06	0.51	0.057
Total (clear plus cloudy) sky (instantaneous)	8.9	0.37	0.09	0.46	0.052
Total sky (base case, FDH)	8.9	0.34	0.09	0.43	0.048
Total sky (upper estimate, FDH)	15.1	0.62	0.15	0.77	0.050
		Present to 2050			
Total sky	5.7	0.21	0.05	0.26	0.047
		Preindustrial to Present (Previous Work)			
Chalita et al. [1996][b]	...	0.22	0.07	0.28	...
Berntsen et al. [1997] (Reading model)	7.6	0.21	0.07	0.28	0.037
Stevenson et al. [1998]	8.7	0.20	0.09	0.29	0.033
Berntsen et al. [1997] (Oslo model)	7.6	0.23	0.08	0.31	0.041
Haywood et al. [1998]	7.9	0.23	0.08	0.31	0.039
Kiehl et al. [1999]	8.4	0.25	0.07	0.32	0.038
Berntsen et al. [2000]	9.6	0.25	0.10	0.34	0.036
Brasseur et al. [1998a]	...	0.25	0.12	0.37	...
van Dorland et al. [1997]	8.1	0.30	0.08	0.38	0.047
Roelofs et al. [1997, 1998]	7.2	0.29	0.13	0.42	0.058
Lelieveld and Dentener [2000]	...	...	...	0.42	...
Mickley et al. [1999][b]	12.6	0.35	0.09	0.44	0.035
Lelieveld and van Dorland [1995][b]	...	...	...	0.49	...

[a]Units are in W m^{-2}. DU, total tropospheric ozone change in Dobson units; LW, longwave radiative forcing; SW, shortwave radiative forcing; total, total radiative forcing; normalized, normalized radiative forcing in W m^{-2} DU^{-1}.
[b]No stratospheric temperature adjustment applied.

(SW plus LW) forcing reaches a maximum value of 1 W m^{-2} over the Sahara region. In the northern hemisphere where the ozone increase is maximum, the forcing ranges from about 0.4-0.5 W m^{-2} to 0.6-0.8 W m^{-2} in the subtropics. In the southern hemisphere a maximum reaching 0.7 W m^{-2} and associated primarily with biomass burning emissions is predicted in the subtropics. At higher latitudes a much lower forcing is derived. The calculated global and total (SW plus LW) forcing is 0.43 W m^{-2} (Table 4). As far as the geographical distribution of the forcing is concerned, we find a fairly good agreement with previous modeling work, in particular, concerning the maximum over Sahara [*Berntsen et al.*, 1997; *Roelofs et al.*, 1997; *van Dorland et al.*, 1997; *Mickley et al.*, 1999]. A somewhat different picture has been presented by *Kiehl et al.* [1999] on the basis of observed ozone distributions. In their study, no maximum is found over the Sahara. The high shortwave forcing calculated in the present study for the Arctic is in particular good agreement with the estimate by *Mickley et al.* [1999].

The global mean forcings are in the range given by previous estimates calculated with global 3-D models (Table 4). The tropospheric O_3 SW forcing is in the range 0.07-0.09 W m^{-2}, except in the case of two specific studies [*Roelofs et al.*, 1997; *Brasseur et al.*, 1998a], which report a higher value of 0.12 W m^{-2}. A problem with daytime averaging is responsible for the higher value reported by *Brasseur et al.* [1998a] (T. Schneider, personal communication, 2000). The disagreement obtained with the *Roelofs et al.* [1997] value is unclear. The global LW forcing from previous studies ranges from 0.20 to 0.35 W m^{-2}. This value is subject to larger variability among the various estimates associated with radiation code properties (in particular the ozone 14 micron band or the spectral resolution) [e.g., *Shine et al.*, 1995], climatologies used for temperature, water vapor, and clouds [*Haywood et al.*, 1998; *Roelofs*, 1999], ozone change itself and shape of the ozone profile around the tropopause [*Shine and Forster*, 1999; *Kiehl et al.*, 1999], or the stratospheric temperature adjustment. The total forcing provided by previous model studies ranges from 0.28 to 0.49 W m^{-2}. We note, however, that several model simulations [e.g., *Chalita et al.*, 1996; *Mickley et al.*, 1999] did not apply a stratospheric temperature adjustment and others [*Lelieveld and van Dorland*, 1995] considered clear-sky conditions only. In our calculations the stratospheric temperature adjustment tends to reduce the instantaneous total forcing by 8% (Table 4). This figure is close to the results of *Haywood et al.* [1998], who calculated a decrease of 9%. A larger effect of 18–20% has been obtained by *Berntsen et al.* [1997]. In their model the effect of clouds is to reduce the total forcing by 17% (Table 4), in the range of previous estimates of this effect [*Berntsen et al.*, 1997; *Haywood et al.*, 1998; *Kiehl et al.*, 1999; *Roelofs et al.*,

1998]. The global mean forcing calculated in this study (0.43 W m^{-2}) is on the high side of this range.

As discussed earlier, there is a high uncertainty on calculated preindustrial ozone levels. Several models, for example, have difficulties to simulate the low ozone concentrations reported over Europe at the end of the nineteenth century [*Roelofs et al.*, 1997; *Wang and Jacob*, 1998; *Berntsen et al.*, 2000; *Mickley et al.*, 1999]. As shown earlier, the preindustrial levels are strongly influenced by the assumptions made regarding natural emissions (i.e., NO soil emissions, lightning, preindustrial biomass burning). The calculated ozone forcing is particularly sensitive to the estimated preindustrial background concentrations used in the models [*Mickley et al.*, 2001]. A large uncertainty is associated with the assumptions made for biomass burning emissions during the preindustrial era. By assuming that these emissions were 20% of their present values at all locations including the boreal regions where fires are generally triggered by lightning and have probably been as frequent and as intense as today, our preindustrial ozone levels at high northern latitudes may be underestimated. To illustrate the role played by different preindustrial ozone levels on the calculation of the radiative forcing, an additional calculation has been performed in which the so-called stratospheric ozone tracer is considered to represent the preindustrial levels. As discussed earlier (see Plate 3), this tracer originates from the stratosphere and penetrates into the troposphere where it is destroyed by photochemical loss and dry deposition. This tracer is not affected by in situ photochemical production within the troposphere and therefore provides a lower limit for natural ozone below the tropopause. When this tracer is used as background ozone conditions for preindustrial conditions, the radiative forcing caused by present-day ozone increases to a global mean value of 0.77 W m^{-2} (Table 4). This forcing, 80% larger than our best estimate of the forcing since preindustrial times, indicates that natural emissions of precursors significantly contribute to the photochemical production of ozone in the pristine (and preindustrial) troposphere and to the background level of ozone. Recently, *Mickley et al.* [2001] calculated a forcing of 0.72-0.80 W m^{-2} as a result of various sensitivity simulations regarding natural emissions. Our upper estimate is in agreement with this range.

The seasonal cycle of the total forcing is illustrated on Plate 10. A strong maximum reaching 0.9 W m^{-2} is predicted in summer at northern midlatitudes and is associated with intense ozone photochemical production in polluted regions. A second maximum reaching more than 0.9 W m^{-2} and associated with a maximum in the SW forcing is also calculated in the Arctic in July during the polar day. In the subtropics the forcing is larger than 0.5 W m^{-2} in both hemispheres. The seasonal cycle agrees well with the results of *Mickley et al.* [1999], in particular regarding the shortwave forcing calculated in June-July in the Arctic.

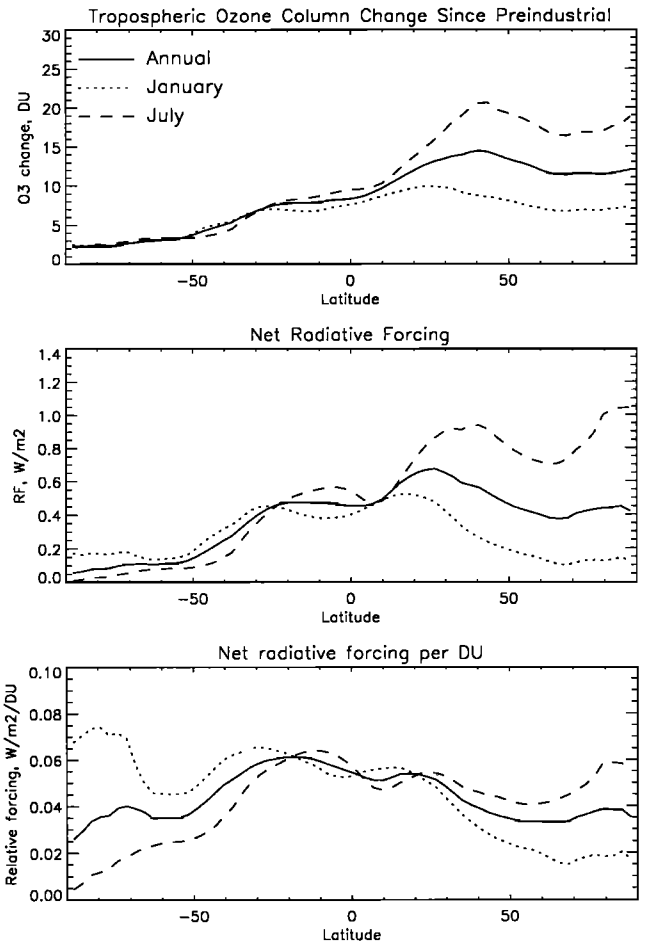

Figure 3. Latitudinal variation of (top) tropospheric ozone column change since the preindustrial period (DU), (middle) radiative forcing at the tropopause (W m^{-2}), and (bottom) normalized forcing (W m^{-2} DU^{-1}). Solid line, annual mean; dotted line, January; dashed line, July.

Figure 3 shows the zonally averaged change in tropospheric ozone column, the radiative forcing, and the normalized forcing (forcing divided by the ozone tropospheric column change). The radiative forcing ranges from 0.05 W m^{-2} in the southern hemisphere to a maximum of about 1 W m^{-2} in the subtropics in the northern hemisphere during summer. As expected, the radiative forcing is larger in the northern hemisphere where most of the ozone increase took place. The normalized forcing shows lower variability and ranges from 0.03 W m^{-2} DU^{-1} in annual mean at high latitudes to a value fairly constant throughout the year of 0.06 W m^{-2} DU^{-1} in the in the tropics and subtropics. A global mean normalized forcing of 0.048 W m^{-2} DU^{-1} is calculated for total sky conditions.

4. Future Evolution (2050) Under IPCC IS92a Scenario

The surface ozone calculated for 2050 (based on IS92a scenario of IPCC) is shown on Plate 11 for both Jan-

uary and July conditions along with the corresponding relative change from present-day distribution (2050 divided by present-day O_3 mixing ratio). The future ozone increase occurs mainly in the tropics where rapid economic growth and population increase are expected. The simulated ozone increase reaches maximum values of 60-80% in Southeast Asia, India, and Central America during all seasons. In these regions, ozone mixing ratios reaching 50-60 ppbv are calculated. In January, an important ozone outflow from Asia toward the Pacific and northern United States is predicted, with mixing ratios of 30-40 ppbv within the plume. Previous work has already indicated the importance of pollutant export from Southeast Asia for global scale ozone levels in the future [*Berntsen et al.*, 1996, 1999; *Jacob et al.*, 1999]. During the austral summer, surface ozone also increases by 50-70% in South America and South Africa, reaching monthly mean mixing ratios of 45-50 ppbv. Ozone plumes emanating from these regions and transported over large distances over the ocean are also visible. It is important to note that the comparison with the present-day distribution (see Plate 5) shows an increase in background ozone in the southern hemisphere with mixing ratios of 25-30 ppbv in remote oceanic regions. Unlike the ozone evolution from the preindustrial era which occured mainly at northern midlatitudes, the calculated 2050 distribution suggests that the future evolution will be mainly located in the tropics and subtropics, and in the southern hemisphere.

Plate 12 provides a different perspective on the future ozone change and shows the zonal mean increase (in both percent and ppbv) from present to 2050 for January and July conditions. As illustrated earlier, the ozone increase appears in the tropics during both seasons and reaches 40% in zonal average. Because of rapid upward transport in these regions, the ozone increase propagates through the mid and upper troposphere where the impact on the radiative forcing is the largest. In July an ozone increase reaching 30-35% and associated with convective mixing is predicted in the tropical upper troposphere. Transport from the tropical and subtropical boundary layer to higher latitudes along isentropes is also visible during both seasons. In July, ozone increases by up to 20-25% in the northern hemisphere upper troposphere. Again, this future evolution clearly contrasts with the ozone increase from the preindustrial era (see Plate 7) mainly located at northern midlatitudes. The calculated ozone change is in general agreement with the previous estimate by *Brasseur et al.* [1998a], who used the IS92a scenario without changing the geographical distribution of the emissions. We note that, as a consequence, the change in ozone is less marked in the southern hemisphere in this earlier study.

As a consequence of increased surface emissions and photochemical production, the global burden of CO increases by 40% from present to 2050 (Table 2). The global CO photochemical lifetime increases by about 5 days (from 1.97 to 2.15 months), and the methane photochemical lifetime increases by about 1 year (from 9.28 to 10.21), reflecting a 10% reduction in the global mean OH concentration and, hence a decrease in the oxidizing power of the atmosphere. The tropospheric ozone global net photochemical production increases by about 40% from present to future (Table 3), and the global ozone burden increases by about 22% (46 Tg). It should be noted that these future estimates are highly uncertain and should only be used as an illustration of the potential evolution of ozone in the future. However, it is important to emphasize that these future estimates reveal the crucial role played by the emissions in countries subject to rapid economic and population growths, especially countries located in the tropics.

The future ozone change has been introduced in the radiation model in order to calculate the climate forcing. The annual mean total forcing (Plate 13) shows high values in the subtropical band in the northern hemisphere in the range 0.4-0.6 W m^{-2}, peaking at 0.65 W m^{-2} over regions with high albedo (i.e., South Arabian peninsula). Secondary maxima of 0.35 W m^{-2} are also predicted in the southern tropics over the Atlantic and Indian Oceans. The global mean forcing is 0.26 W m^{-2} (see Table 4). On the basis of this model estimate the radiative forcing of tropospheric ozone in 2050 (from a preindustrial atmosphere) reaches 0.69 W m^{-2} in global and annual mean. It is difficult to compare these numbers with previous estimates which used different assumptions regarding future scenarios and reference years. A first estimate of the future forcing by *Chalita et al.* [1996] provided a global forcing of 0.15 W m^{-2} from present to 2050 based on IS92a. On the basis of a similar scenario, *van Dorland et al.* [1997] and *Brasseur et al.* [1998a] reported forcings of 0.28 and 0.26 W m^{-2}, respectively. Our new estimate is therefore fairly close to these two values.

5. Conclusions

In this study, we have used the MOZART global chemical-transport model to investigate the tropospheric ozone evolution since the preindustrial period and in the future (2050) associated with increasing anthropogenic emissions of precursors (CH_4, CO, NO_x, NMHCs). Ozone has increased by more than a factor of 3 since the preindustrial era at northern midlatitudes where anthropogenic emissions are important. Comparisons of the model results with surface ozone measurements recorded during the nineteenth century are generally consistent at midlatitudes over Europe, showing mixing ratios of about 10 ppbv, with little variation throughout the year. The preindustrial ozone levels appear to be very sensitive to assumptions made for natural emissions. In particular, NO_x soil emissions have increased by a factor of 2 due to fertilizer use. This particular emission represents the main surface source of NO_x at these latitudes for pristine conditions, and assumptions

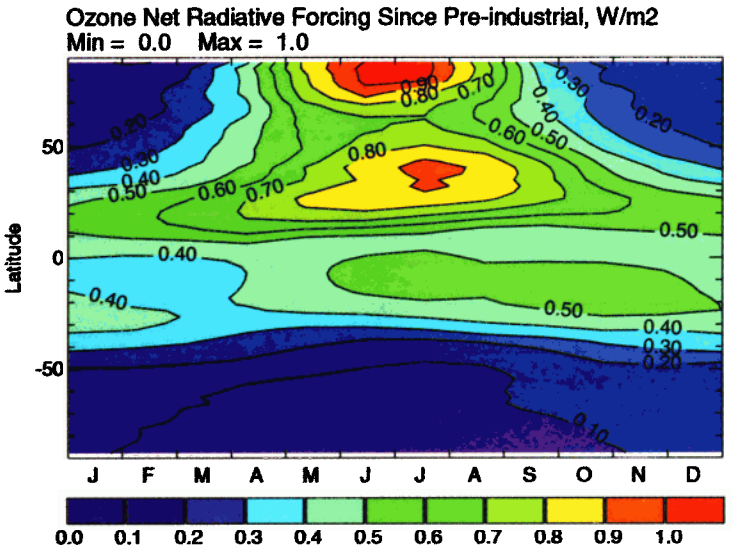

Plate 10. Seasonal cycle of the zonal mean tropospheric ozone total radiative forcing since the preindustrial period as a function of latitude (W m^{-2}).

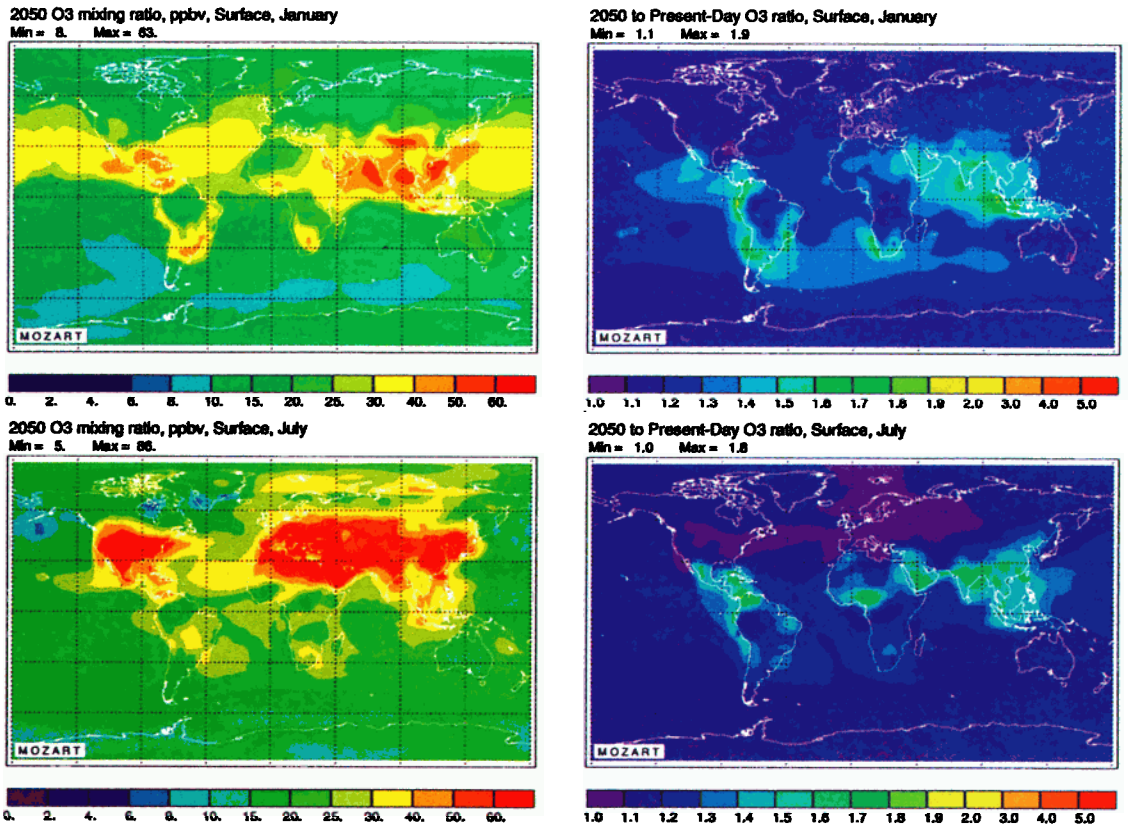

Plate 11. (left) Distribution of surface ozone mixing ratio (ppbv) calculated in January and July for 2050 conditions, and (right) corresponding relative increase from present.

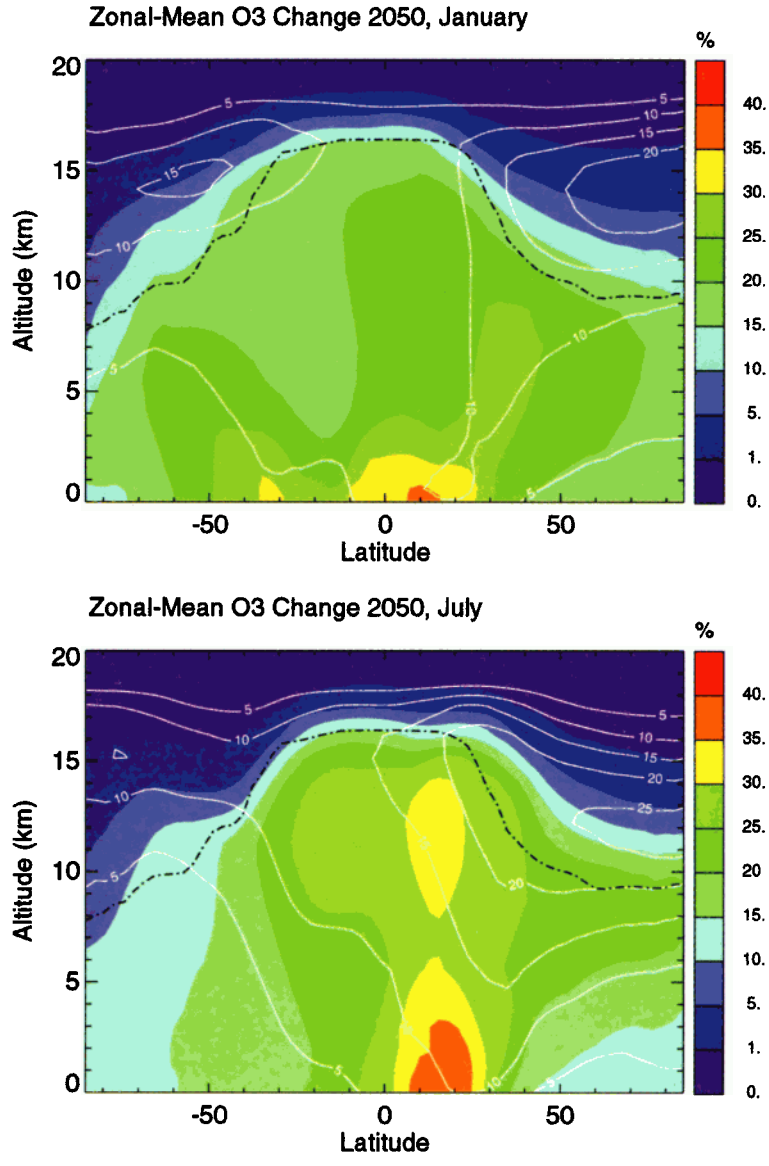

Plate 12. Zonal mean change in ozone from present to 2050 for January and July conditions. Shaded contours give the change in percent, and solid contours give the increase in ppbv.

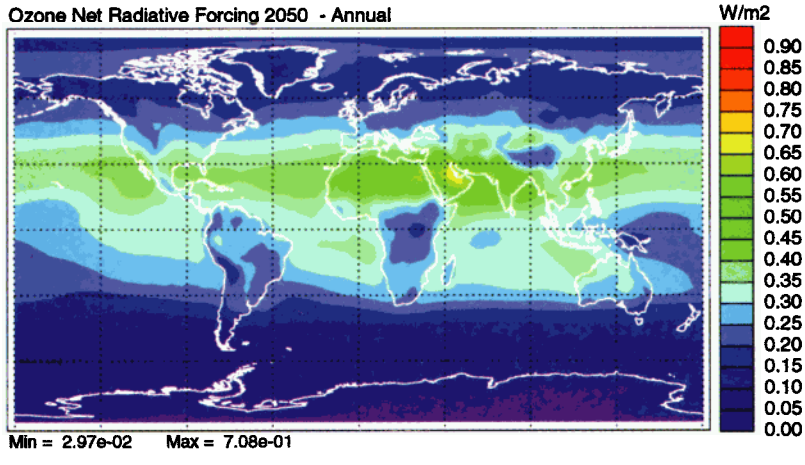

Plate 13. Annual mean tropospheric ozone total forcing at the tropopause calculated from present to 2050 (W m^{-2}).

on their preindustrial level are crucial regarding simulated surface ozone. The situation is also complex in tropical regions where recorded preindustrial ozone levels at the surface indicate very low values of only 5 ppbv. Confidence in measured ozone levels is, however, limited due to artifacts associated with the technique used at that time. In particular, ambient humidity affects the ozone readings, and this error is potentially important in the tropics. In addition, it is clear that calculated ozone levels in the tropics crucially depend on assumptions made for biomass burning emissions of precursors (strength and geographical distribution) and lightning emissions of NO_x.

The simulated future evolution (year 2050 according to IPCC IS92a scenario) suggests that surface ozone is likely to increase in regions where rapid economic growth and population increase are expected. This is particularly the case in the northern subtropical region where increased photochemical production of ozone by enhanced emissions in Southeast Asia and Central America and subsequent export by long-range transport affects the whole subtropical band. This transport also affects northern midlatitudes (northern United States, Europe) to some extent. However, in these regions, decreased emissions due to regulation measures compensate, and a limited ozone increase is predicted. Our results also indicate that the potential future evolution will also significantly affect the background levels of ozone in the most pristine regions of the troposphere. In particular, ozone concentrations higher by 10-20% are calculated over marine regions in the southern hemisphere. Owing to rapid upward transport in the tropics, in particular by convection, ozone and other pollutants propagate efficiently from the boundary layer up to the upper troposphere. This feature is of particular importance since the tropical upper troposphere is the most sensitive region as far as the ozone greenhouse effect is concerned.

We have used the modeled changes in ozone distribution to calculate the associated radiative forcing of climate. Our best estimate of the tropospheric O_3 radiative forcing since the preindustrial period is 0.43 W m^{-2} (global and annual mean). This value represents about 20% of the radiative forcing associated with the well-mixed greenhouse gases (2.42 W m^{-2}). In contrast to well-mixed greenhouse gas forcing (CO_2, CH_4, N_2O, halogens), the O_3 forcing shows a strong spatial heterogeneity with a maximum in the subtropics and a strong seasonal cycle peaking during summer. The O_3 forcing is particularly sensitive to the assumed preindustrial level of ozone. An upper estimate on our forcing is calculated by assuming preindustrial ozone levels in the troposphere affected only by exchanges with the stratosphere (no tropospheric photochemical source/sinks). In this case the calculated forcing is 0.77 W m^{-2}. This emphasizes the important role played by natural emissions of ozone precursors (biogenic, lightning, oceans) in the calculation of preindustrial ozone levels. In 2050 an additional forcing of 0.26 W m^{-2} is obtained, providing an ozone forcing from preindustrial to 2050 is 0.69 W m^{-2}. A global mean normalized forcing of 0.048 W m^{-2} DU^{-1} is calculated for total sky conditions.

Finally, we would like to emphasize two important limitations of this work. First, the ozone evolution presented in this study only considers the role played by increasing emissions of precursors. This allows us to isolate this particular effect on the composition of the troposphere. However, other factors are likely to play an important role in determining the tropospheric ozone change in an evolving climate system. In particular, changes in climate (i.e., water vapor, temperature, dynamics, clouds, precipitations, convective regime) are likely to have influenced (and influence in the future) the budget of tropospheric ozone. Furthermore, the influence of stratospheric ozone change and its influence on both tropospheric chemistry through penetration of ultraviolet radiation and export to the lower atmosphere is not taken into account in the present study. Second, scenarios for future evolution are highly uncertain. In this study, we use the IPCC IS92a as a reference scenario. New scenarios are currently being prepared for the IPCC third assessment report considering more recent assumptions affecting economical growth and regulatory measures. Even with these updated emissions, the prediction of a future evolution remains highly speculative. Therefore the model predictions reported here should be considered only as an illustration of potential development of ozone and precursors in the future.

Acknowledgments. We gratefully thank J. Yienger, H. Levy, and A. Klonecki for providing us with the updated NO soil emissions. Thanks to J. Kiehl, T. Schneider, and C. Zender for making the NCAR Column Radiation Model available to our use and for adapting their model to the MOZART output. Helpful discussions, and comments on this work by S. Solomon are particularly appreciated. Thanks to S. Walters for his continuous help with the MOZART model development. The National Center for Atmospheric Reasearch is sponsored by the National Science Foundation.

References

Andreae, M. O., E. Atlas, H. Cachier, W. R. Cofer III, G. W. Harris, G. Helas, R. Koppmann, J.-P. Lacaux, and D. E. Ward, Trace gas and aerosol emissions from savanna fires, in *Biomass Burning and Global Change*, vol. 1, edited by J. S. Levine, pp. 278-295, MIT Press, Cambridge, Mass., 1996.

Anfossi, D., S. Sandroni, and S. Viarengo, Tropospheric ozone in the nineteenth century: The Moncalieri series, *J. Geophys. Res.*, *96*, 17,349-17,353, 1991.

Berntsen, T. K., I. S. A. Isaksen, W.-C. Wang, and Z.-X. Liang, Impact of increased anthropogenic emissions in Asia on tropospheric ozone and climate, *Tellus*, *Ser. B*, 48, 13-32, 1996.

Berntsen, T. K., I. S. A. Isaksen, G. Myhre, J. S. Fuglestvedt, F. Stordal, T. Alsvik Larsen, R. S. Freckleton, and K. P. Shine, Effects of anthropogenic emissions on

tropospheric ozone and its radiative forcing, *J. Geophys. Res.*, *102*, 28,101-28,126, 1997.

Berntsen, T. K., S. Karlsdottir, and D. A. Jaffe, Influence of Asian emissions on the composition of air reaching the North Western United States, *Geophys. Res. Lett.*, *26*, 2171-2174, 1999.

Berntsen, T. K., G. Myhre, F. Stordal, and I. S. A. Isaksen, Time evolution of tropospheric ozone and its radiative forcing, *J. Geophys. Res.*, *105*, 8915-8930, 2000.

Bojkov, R. D., Surface ozone during the second half of the nineteenth century, *Mon. Weather Rev.*, *25*, 343-352, 1986.

Brasseur, G. P., D. A. Hauglustaine, and S. Walters, Chemical compounds in the remote Pacific troposphere: Comparison between MLOPEX measurements and chemical transport model calculations, *J. Geophys. Res.*, *101*, 14,795-14,813, 1996.

Brasseur, G. P., X. X. Tie, P. J. Rasch, and F. Lefèvre, A three-dimensional simulation of the Antarctic ozone hole: Impact of anthropogenic chlorine on the lower stratosphere and upper troposphere, *J. Geophys. Res.*, *102*, 8909-8930, 1997.

Brasseur, G. P., J. T. Kiehl, J.-F. Müller, T. Schneider, C. Granier, X. X. Tie, and D. Hauglustaine, Past and future changes in global tropospheric ozone: Impact on radiative forcing, *Geophys. Res. Lett.*, *25*, 3807-3810, 1998a.

Brasseur, G. P., D. A. Hauglustaine, S. Walters, P. J. Rasch, J.-F. Müller, C. Granier, and X. X. Tie, MOZART, a global chemical transport model for ozone and related chemical tracers, 1, Model description, *J. Geophys. Res.*, *103*, 28,265-28,289, 1998b.

Briegleb, B. P., Delta-Eddington approximation for solar radiation in the NCAR Community Climate Model, *J. Geophys. Res.*, *97*, 7603-7612, 1992.

Chalita, S., D. A. Hauglustaine, H. Le Treut, and J.-F. Müller, Radiative forcing due to increased tropospheric ozone concentrations, *Atmos. Environ.*, *30*, 1641-1646, 1996.

Crutzen, P. J., and P. H. Zimmermann, The changing photochemistry of the troposphere, *Tellus*, *43*, 136-151, 1991.

Dickinson, R. E., and R. J. Cicerone, Future global warming from atmospheric trace gases, *Nature*, *319*, 109-115, 1986.

Emmons, L. K., et al., Climatologies of NO_x and NO_y: A comparison of data and models, *Atmos. Environ.*, *31*, 1851-1904, 1997.

Emmons, L. K., D. A. Hauglustaine, J.-F. Müller, M. A. Carroll, G. P. Brasseur, D. Brunner, J. Stahelin, V. Thouret, and A. Marenco, Data composites of airborne observations of tropospheric ozone and its precursors, *J. Geophys. Res.*, *105*, 20,497-20,538, 2000.

Fishman, J., The global consequences of increasing tropospheric ozone concentrations, *Chemosphere*, *22*, 685-695, 1991.

Fishman, J., V. Ramanathan, P. J. Crutzen, and S. C. Liu, Tropospheric ozone and climate, *Nature*, *282*, 818-820, 1979.

Forster, P. M. de F., C. E. Johnson, K. S. Law, J. A. Pyle, and K. P. Shine, Further estimates of radiative forcing due to tropospheric ozone, *Geophys. Res. Lett.*, *23*, 3321-3324, 1996.

Granier, C., W. M. Hao, G. Brasseur, and J.-F. Müller, Land use practices and biomass burning: Impact on the chemical composition of the atmosphere, in *Biomass Burning and Global Change*, Vol. 1., edited J. S. Levine, pp. 140-198, MIT Press, Cambridge, Mass., 1996.

Haan, D., and D. Raynaud, Ice core record of CO variations during the last two millennia: Atmospheric implications and chemical interactions within the Greenland ice, *Tellus*, *50*, 253-262, 1998.

Haan, D., P. Martinerie, and D. Raynaud, Ice core data of atmospheric carbon monoxide over Antarctica and Greenland during the last 200 years, *Geophys. Res. Lett.*, *23*, 2235-2238, 1996.

Hack, J. J., Parameterization of moist convection in the NCAR community climate model (CCM2), *J. Geophys. Res.*, *99*, 5551-5568, 1994.

Hao, W. M., and M.-H. Liu, Spatial distribution of tropical biomass burning in 1980 with $5° \times 5°$ resolution, *Global Biogeochem. Cycles*, *8*, 495-503, 1994.

Hao, W. M., D. E. Ward, G. Olbu, and S. P. Baker, Emissions of CO_2, CO, and hydrocarbons from fires in diverse African savanna ecosystems, *J. Geophys. Res.*, *101*, 23,577-23,584, 1996.

Hauglustaine, D. A., and C. Granier, Radiative forcing by tropospheric ozone changes due to increased emissions of CH_4, CO and NO_x, in *Atmospheric Ozone As a Climate Gas*, edited by W.-C. Wang and I. S. A. Isaksen, pp. 189-203, Springer-Verlag, New York, 1995.

Hauglustaine, D. A., C. Granier, G. P. Brasseur, and G. Mégie, The importance of atmospheric chemistry in the calculation of radiative forcing on the climate system, *J. Geophys. Res.*, *99*, 1173-1186, 1994.

Hauglustaine, D. A., G. P. Brasseur, S. Walters, P. J. Rasch, J.-F. Müller, L. K. Emmons, and M. A. Carroll, MOZART, a global chemical transport model for ozone an and evaluation, *J. Geophys. Res.*, *103*, 28,291-28,335, 1998a.

Hauglustaine, D. A., G. P. Brasseur, and S. Walters, A three-dimensional simulation of ozone over the North Atlantic Ocean, in *Atmospheric Ozone*, edited by R. D. Bojkov and G. Visconti, pp. 735-738, Int. Ozone Comm., L'Aquila, Italy, 1998b.

Hauglustaine, D. A., G. P. Brasseur, and J. S. Levine, A sensitivity simulation of tropospheric ozone changes due to the 1997 Indonesian fire emissions, *Geophys. Res. Lett.*, *26*, 3305-3308, 1999.

Hauglustaine, D. A., L. K. Emmons, M. Newchurch, G. P. Brasseur, T. Takao, K. Matsubara, J. Johnson, B. Ridley, J. Stith, and J. Dye, On the role of lightning NO_x in the formation of tropospheric ozone plumes: A global model perspective, *J. Atmos. Chem.*, *38*, 277-294, 2001.

Haywood, J. M., M. D. Schwarzkopf, and V. Ramaswamy, Estimates of radiative forcing due to modeled increases in tropospheric ozone, *J. Geophys. Res.*, *103*, 16,999-17,007, 1998.

Holtslag, A., and B. Boville, Local versus nonlocal boundary-layer diffusion in a global climate model, *J. Clim.*, *6*, 1825-1842, 1993.

Hoinka, K., Statistics of the global tropopause pressure, *Mon. Weather Rev.*, *126*, 3303-3325, 1998.

Hough, A. M., and R. G. Derwent, Changes in the global concentration of tropospheric ozone due to human activities, *Nature*, *344*, 645-648, 1990.

Intergovernmental Panel on Climate Change (IPCC), *Climate Change: The IPCC Scientific Assessment*, edited by J. T. Houghton, B. A. Callander, and S. K. Varney, Cambridge Univ. Press, New York, 1990.

Intergovernmental Panel on Climate Change (IPCC), *Climate change 1992: The Supplementary Report to the IPCC Scientific Assessment*, edited by J. T. Houghton, B. A. Callander, and S. K. Varney, Cambridge Univ. Press, New York, 1992.

Intergovernmental Panel on Climate Change (IPCC), *Climate Change 1994: Radiative Forcing of Climate Change and an Evaluation of the IPCC IS92 Emission Scenarios*, edited by J. T. Houghton et al., Cambridge Univ. Press, New York, 1994.

Intergovernmental Panel on Climate Change (IPCC), *Cli-*

mate Change 1995: The Science of Climate Change, Contribution of Working Group I to the Second Assessment Report of the IPCC, edited by J. T. Houghton et al., Cambridge Univ. Press, New York, 1996.

Intergovernmental Panel on Climate Change (IPCC), *Aviation and the global atmosphere*, edited by J. E. Penner et al., Cambridge Univ. Press, New York, 1999.

Jacob, D. J., J. A. Logan, and P. P. Murti, Effect of rising Asian emissions on surface ozone in the United States, *Geophys. Res. Lett., 26*, 2175-2178, 1999.

Jaffe, D., et al., Transport of Asian air pollution to North America, *Geophys. Res. Lett., 26*, 711-714, 1999.

Kanakidou, M., et al., 3-D global simulations of tropospheric CO distributions - Results of the GIM/IGAC intercomparison 1997 exercise, *Chemosphere Global Change Sci., 1*, 263-282, 1999a.

Kanakidou, M., et al., 3-D global simulations of tropospheric chemistry with focus on ozone distributions, *EUR 18842*, Eur. Comm., Luxembourg, 1999b.

Kiehl, J. T., and B. P. Briegleb, The relative roles of sulfate aerosols and greenhouse gases in climate forcing, *Science, 260*, 311-314, 1993.

Kiehl, J. T., J. J. Hack, G. B. Bonan, B. A. Boville, D. L. Williamson, and P. J. Rasch, The National Center for Atmospheric Research Community Climate Model: CCM3, *J. Clim., 11*, 1131-1149, 1998.

Kiehl, J. T., T. L. Schneider, R. W. Portmann, and S. Solomon, Climate forcing due to tropospheric and stratospheric ozone, *J. Geophys. Res., 104*, 31,239-31,254, 1999.

Lacis, A. A., D. J. Wuebbles, and J. A. Logan, Radiative forcing of climate by changes in the vertical distribution of ozone, *J. Geophys. Res., 95*, 9971-9981, 1990.

Law, K. S., et al., Comparison between global chemistry transport model results and Measurement of Ozone and Water Vapor by Airbus In-Service Aircraft (MOZAIC) data, *J. Geophys. Res., 105*, 1503-1526, 2000.

Lelieveld, J., and F. J. Dentener, What controls tropospheric ozone?, *J. Geophys. Res., 105*, 3531-3551, 2000.

Lelieveld, J., and R. van Dorland, Ozone chemistry changes in the troposphere and consequent radiative forcing of climate, in *Atmospheric Ozone As a Climate Gas*, edited by W.-C. Wang and I. S. A. Isaksen, pp. 227-258, Springer-Verlag, New York, 1995.

Levy, H., II, P. S. Kasibhatla, W. J. Moxim, A. A. Klonecki, A. I. Hirsch, S. J. Oltmans, and W. L. Chameides, The global impact of human activities on tropospheric ozone, *Geophys. Res. Lett., 24*, 791-794, 1997.

Linvill, D. E., W. J. Hooker, and B. Olson, Ozone in Michigan's environment 1876-1880, *Mon. Weather Rev., 108*, 1883-1891, 1980.

Marenco, A., H. Gouget, P. Nédélec, J.-P. Pagès, and F. Karcher, Evidence of a long-term increase in tropospheric ozone from Pic du Midi data series: Consequences - Positive radiative forcing, *J. Geophys. Res., 99*, 16,617-16,632, 1994.

Mauzerall, D. L., D. Narita, H. Akimoto, L. Horowitz, S. Walters, D. Hauglustaine, and G. Brasseur, Seasonal characteristics of tropospheric ozone production and mixing ratios over East Asia: A global three-dimensional chemical transport model analysis, *J. Geophys. Res., 105*, 17,895-17,910, 2000.

Mickley, L. J., P. P. Murti, D. J. Jacob, J. A. Logan, D. M. Koch, and D. Rind, Radiative forcing from tropospheric ozone calculated with a a unified chemistry-climate model, *J. Geophys. Res., 104*, 30,153-30,172, 1999.

Mickley, L. J., D. J. Jacob, and D. Rind, Uncertainty in preindustrial abundance of tropospheric ozone: Implications for radiative forcing calculations, *J. Geophys. Res., 106*, 3389-3399, 2001.

Müller, J.-F., Geographical distribution and seasonal variation of surface emissions and deposition velocities of atmospheric trace gases, *J. Geophys. Res., 97*, 3787-3804, 1992.

Müller, J.-F., and G. P. Brasseur, IMAGES: A three-dimensional chemical transport model of the global troposphere, *J. Geophys. Res., 100*, 16,445-16,490, 1995.

Pavelin, E. G., C. E. Johnson, S. Rughooputh, and R. Toumi, Evaluation of preindustrial surface ozone measurements made using Schönbein's method, *Atmos. Environ., 33*, 919-929, 1999.

Pepper, W., J. Legett, R. Swart, J. Wasson, J. Edmonds, and I. Mintzer, Emission scenarios for the IPCC an update: Assumptions, methodology, and results, Intergov. Panel on Clim. Change, Working Group I, 1992.

Portmann, R. W., S. Solomon, J. Fishman, J. R. Olson, J. T. Kiehl, and B. Briegleb, Radiative forcing of the Earth-climate system due to tropical tropospheric ozone production, *J. Geophys. Res., 102*, 9409-9417, 1997.

Ramanathan, V., and R. E. Dickinson, The role of stratospheric ozone in the zonal and seasonal radiative energy balance of the Earth-troposphere system, *J. Atmos. Sci., 36*, 1084-1104, 1979.

Ramanathan, V., R. J. Cicerone, H. B. Singh, and J. T. Kiehl, Trace gas trends and their potential role in climate change, *J. Geophys. Res., 90*, 5547-5566, 1985.

Roelofs, G.-J., Radiative forcing by tropospheric ozone: Impact of cloud representation, *Geophys. Res. Lett., 26*, 467-470, 1999.

Roelofs, G.-J., and J. Lelieveld, Model study of the influence of cross-tropopause O_3 transports on tropospheric O_3 levels, *Tellus, Ser. B, 49*, 38-55, 1997.

Roelofs, G.-J., J. Lelieveld, and R. van Dorland, A three-dimensional chemistry/general circulation model simulation of anthropogenically derived ozone in the troposphere and its radiative climate forcing, *J. Geophys. Res., 102*, 23,389-23,401, 1997.

Roelofs, G.-J., J. Lelieveld, and J. Feichter, Model simulations of the changing distribution of ozone and its radiative forcing of climate: Past, present, and future, *rep. 282*, Max Planck Inst. für Meteorol., Hamburg, Germany, 1998.

Sandroni, S., and D. Anfossi, Historical data of surface ozone at tropical latitudes, *Sci. Total Environ., 148*, 23-29, 1994.

Sandroni, S., D. Anfosi, and S. Viarengo, Surface ozone levels at the end of the nineteenth century in South America, *J. Geophys. Res., 97*, 2535-2539, 1992.

Shine, K. P., and P. M. de F. Forster, The effect of human activity on radiative forcing of climate change: A review of recent developments, *Global Planet. Change, 20*, 205-225, 1999.

Shine, K. P., B. P. Briegleb, A. S. Grossman, D. Hauglustaine, H. Mao, V. Ramaswamy, M. D. Schwarzkopf, R. van Dorland, and W.-C. Wang, Radiative forcing due to changes in ozone: a comparison of different codes, in *Atmospheric Ozone As a Climate Gas*, edited by W.-C. Wang and I. S. A. Isaksen, pp. 373-396, Springer-Verlag, New York, 1995.

Stevenson, D. S., C. E. Johnson, W. J. Collins, R. G. Derwent, K. P. Shine, and J. M. Edwards, Evolution of tropospheric ozone radiative forcing, *Geophys. Res. Lett., 25*, 3819-3822, 1998.

Stevenson, D. S., C. E. Johnson, W. J. Collins, R. G. Derwent, and J. M. Edwards, Future estimates of tropospheric ozone radiative forcing and methane turnover - The impact of climate change, *Geophys. Res. Lett., 27*, 2073-2076, 2000.

van Aardenne, J. A., G. R. Carmichael, H. Levy II, D.

Streets, and L. Hordijk, Anthropogenic NO_x emissions in Asia in the priod 1990-2020, *Atmos. Environ., 33*, 633-646, 1999.

van Dorland, R., F. J. Dentener, and J. Lelieveld, Radiative forcing due to tropospheric ozone and sulfate aerosols, *J. Geophys. Res., 102*, 28,079-28,100, 1997.

Volz, A., and D. Kley, Evaluation of the Montsouris series of ozone measurements made in the nineteenth century, *Nature, 332*, 240-242, 1988.

Wang, W.-C., and N. D. Sze, Coupled effects of atmospheric N_2O and O_3 on the Earth's climate, *Nature, 286*, 589-590, 1980.

Wang, Y., and D. J. Jacob, Anthropogenic forcing on tropospheric ozone and OH since preindustrial times, *J. Geophys. Res., 103*, 31,123-31,135, 1998.

Williamson, D. L., and P. J. Rasch, Two-dimensional semi-Lagrangian transport with shape preserving interpolation, *Mon. Weather Rev., 117*, 102-129, 1989.

Yienger, J. J., and H. Levy II, Empirical model of global soil-biogenic NO_x emissions, *J. Geophys. Res., 100*, 11,447-11,464, 1995.

G. P. Brasseur, Max Planck Institute for Meteorology, Bundesstrasse 55, 20146, Hamburg, Germany. (brasseur@dkrz.de)

D. A. Hauglustaine, Laboratoire des Sciences du Climat et de l'Environnement, Laboratoire Mixte CEA-CNRS, Orme des Merisiers, 91191 Gif-sur-Yvette CEDEX, France. (hauglustaine@cea.fr)

(Received October 6, 2000; revised February 19, 2001; accepted March 6, 2001.)